DOI:
10.1172/jci.insight.126315

Document Version
Peer reviewed version

JCI insight

Prelamin A mediates inflammation in dilated and HIV associated cardiomyopathies

Daniel Brayson, … , Ajay M. Shah, Catherine M. Shanahan

JCI Insight. 2019. https://doi.org/10.1172/jci.insight.126315.

Research In-Press Preview AIDS/HIV Cardiology

Graphical abstract

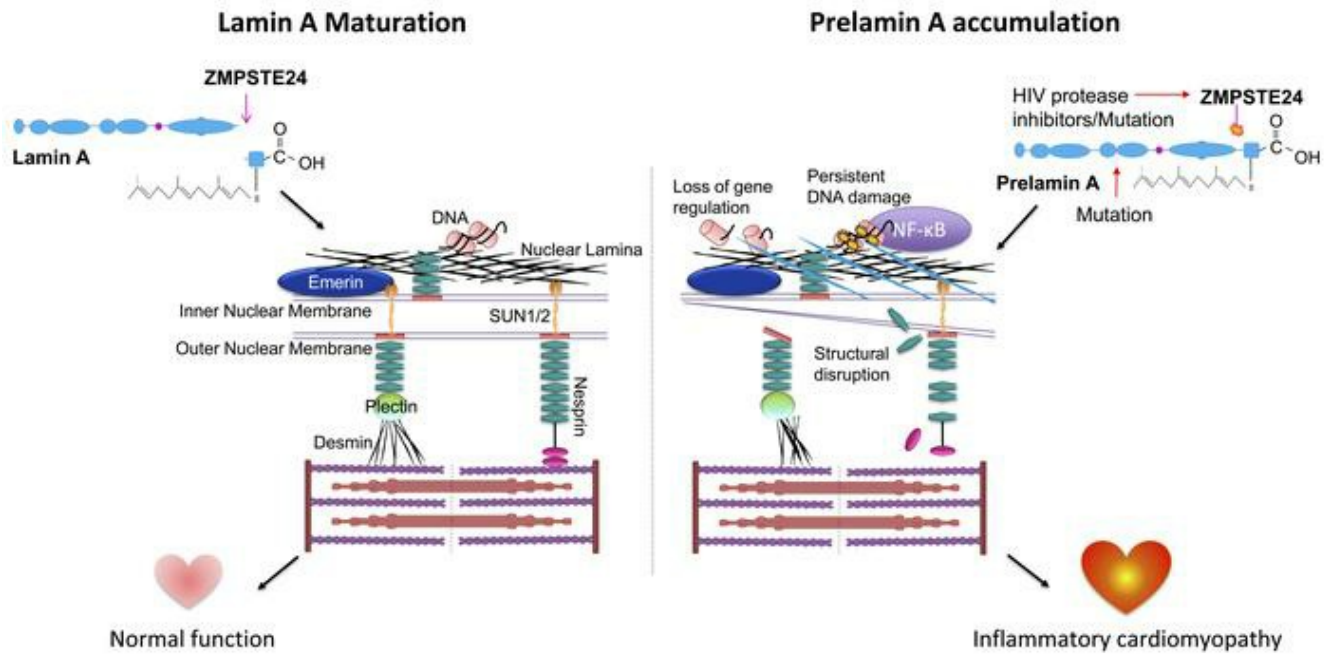

Find the latest version:

http://jci.me/126315/pdf

Prelamin A mediates myocardial inflammation in dilated and HIV associated cardiomyopathies

Authors: Daniel Brayson, PhD[1]; Andrea Frustaci, MD[2,3]; Romina Verardo, PhD[3]; Cristina Chimenti, MD PhD[2,3]; Matteo Antonio Russo, MD[4]; Robert Hayward, BSc[1]; Sadia Munir Ahmad, MSc[1]; Gema Vizcay-Barrena, PhD[5], Andrea Protti, PhD[1]; Peter S. Zammit, PhD[6], Cristobal G. dos Remedios, PhD[7]; Elisabeth Ehler, PhD[1,6]; Ajay M. Shah, MD[1]; Catherine M. Shanahan, PhD[1]

Addresses:

[1]School of Cardiovascular Medicine and Sciences, King's College London BHF Centre for Research Excellence, London, UK

[2]Department of Cardiovascular, Nefrologic, Anestesiologic and Geriatric Sciences, La Sapienza University of Rome, Italy.

[3]National Institute for Infectious Diseases IRCCS 'L. Spallanzani', Rome, Italy

[4]MEBIC Open University San Raffaele and IRCCS San Raffaele Pisana, Laboratory of Molecular and Cellular Pathology, Milan, Italy

[5]Centre for Ultrastructural Imaging, Guy's Campus, King's College London, London, UK

[6]Randall Centre for Cell and Molecular Biophysics, King's College London, UK

[7]Department of Anatomy, Bosch Institute, University of Sydney, Sydney, NSW, Australia

Working Title: Brayson et al., Accumulation of prelamin A in cardiomyopathy

Conflict of interest: The authors declare no conflict of interest

Address for correspondence: Molecular Neurosciences
UCL Great Ormond Street Institute of Child Health
30 Guilford Street
London WC1N 1EH

Telephone: +442078485223

Email: d.brayson@ucl.ac.uk

Abstract

Cardiomyopathies are complex heart muscle diseases that can be inherited or acquired. Dilated cardiomyopathy can result from mutations in *LMNA*, encoding the nuclear intermediate filament proteins lamin A/C. Some *LMNA* mutations lead to accumulation of the lamin A precursor, prelamin A, which is disease causing in a number of tissues yet its impact upon the heart is unknown. Here we discovered myocardial prelamin A accumulation occurred in a case of dilated cardiomyopathy and show that a novel mouse model of cardiac specific prelamin A accumulation exhibited a phenotype consistent with 'inflammatory cardiomyopathy' which we observed to be similar to HIV associated cardiomyopathy, an acquired disease state. Numerous HIV protease therapies are known to inhibit ZMPSTE24, the enzyme responsible for prelamin A processing, and we confirmed that accumulation of prelamin A occurred in HIV+ patient cardiac biopsies. These findings: (1) confirm a unifying pathological role for prelamin A common to genetic and acquired cardiomyopathies; (2) have implications for the management of HIV patients with cardiac disease suggesting protease inhibitors should be replaced with alternative therapies i.e. non-nucleoside reverse transcriptase inhibitors; and (3) suggest that targeting inflammation may be a useful treatment strategy for certain forms of inherited cardiomyopathy.

Key words: Heart Failure, Cardiomyopathy, HIV, Prelamin A, Inflammation, Senescence.

Introduction

Mutations in the *LMNA* gene are commonly implicated in dilated cardiomyopathy (DCM) phenotypes (1), accounting for approximately 6% of all cases (2). Investigation of *in vivo* mouse models harbouring *LMNA* mutations associated with clinical DCM have identified a number of mechanisms associated with disease (3). However, some questions remain unresolved, in particular, whether the lamin A precursor, prelamin A is involved in the pathogenesis of cardiomyopathies (4-7).

The *LMNA* gene produces two distinct proteins, lamin A and lamin C, which together with the B-type lamins form the nuclear lamina which sits adjacent to the inner nuclear membrane (INM) of the nuclear envelope (NE), on the nucleoplasmic side (8). The primary role of the lamina is to provide structural stability to the nuclear environment and to anchor heterochromatin, thereby facilitating appropriate gene expression and efficient DNA damage repair (9, 10). Additionally, the lamina forms part of the linker of nucleoskeleton to cytoskeleton (LINC) complex, which mediates physical communication with the cytoplasmic environment enabling rapid responses to physical cues, a process termed mechanotransduction (11).

To achieve lamin A maturation, its precursor prelamin A, requires step-wise proteolytic processing (12). After translation, addition of farnesyl and carboxymethyl groups to a CAAX motif in the C terminus occurs, followed by an upstream cleavage exclusively mediated by zinc metalloproteinase STE24 homologue, ZMPSTE24, to yield mature lamin A (13-16). Retention of this farnesylated C terminal domain by lamin A precursors is pathologic and mutations in both the *LMNA* and *ZMPSTE24* genes that cause this retention are implicated in premature ageing disorders, such as Hutchinson Gilford progeria syndrome (HGPS), as well as DCM. HGPS patients develop cardiomegaly, atrial enlargement and age-dependent diastolic and systolic dysfunction and left ventricle (LV) hypertrophy (17-19), while the DCM causing mutation *LMNA*-R89L has been shown to result in aberrant processing and accumulation of prelamin A (5, 7). Moreover, a mutation in *LMNA* postulated to inhibit prelamin A processing which causes Dunnigan-type familial lipodystrophy, is also associated with cardiac dysfunction, with patients homozygous for this mutation having worse left ventricle (LV) function indicating a dose-dependent effect (4). Additionally a

mutation in *ZMPSTE24* known to confer a reduction in enzyme activity was found in a patient with metabolic syndrome and cardiomyopathy (6).

Another cause of prelamin A accumulation is via the pharmacological inhibition of ZMPSTE24 activity by Human Immunodeficiency Virus Protease Inhibitors (HIV PIs) used in the treatment of HIV. HIV PIs result in prelamin A accumulation in cells and potentially contribute to adverse effects (20, 21). HIV patients have double the risk for developing cardiovascular disease than non-carriers (22). Moreover, HIV patients can develop HIV-associated cardiomyopathy (23), though the aetiology is complex (24). Previous studies have identified nucleoside reverse transcriptase inhibitors (NRTIs) used in conjunction with HIV PIs as responsible for the development of cardiomyopathy in HIV patients (25, 26). Presently, there is limited knowledge on the impact of HIV PIs on the development of cardiomyopathy though there is an attempt to 'characterise heart function on antiretroviral therapy' with the introduction of the CHART study (27). These points considered, we sought to investigate the extent and effects of prelamin A accumulation in the setting of cardiomyopathy.

Results

Prelamin A can accumulate in DCM patient myocardium

Immunofluorescence staining for prelamin A was performed on human DCM patient LV samples (Supp. Table 1) and non-failing (NF) control samples (Supp. Table 2), and quantified (Fig. 1A,B). Sporadic and focal expression of prelamin A was observable in cardiomyocyte (CM) nuclei in both non-failing and DCM samples. However, in one DCM sample (DCM05) consistent CM nuclear rim staining was found in 71.5% of total CM nuclei. Unfortunately there was no remaining tissue to perform Western blotting on the sample expressing prelamin A, however Western blotting blotting of a selection of the same samples supported the findings that generally prelamin A was not abundant across NF or DCM samples (Fig 1C).

Prelamin A accumulation in cardiomyocytes of mice causes cardiomyopathy and premature death by heart failure

To examine the effects of prelamin A on the heart cardiomyocyte specific prelamin A transgenic (csPLA-Tg) mice were generated. csPLA-Tg mice (Fig. 2A) were born in a normal Mendelian ratio and were indistinguishable from floxed control (FLctrl) mice at birth. Western blotting confirmed that accumulation of prelamin A in csPLA-Tg mice was specific to the heart (Fig. 2B) and immunofluorescence showed that this occurred specifically in the nuclear rim of CMs (Fig. 2C).

After weaning (day 21) csPLA-Tg mice ceased to grow and died prematurely. By 32 days, body weight was significantly lower in csPLA-Tg mice (Fig. 2D) and median survival was significantly attenuated in male and female mice compared with FLctrl (Fig. 2E).

At two weeks csPLA-Tg mice showed no change in structural, dimensional or functional parameters by echocardiography as compared to FLctrl controls (Fig. 3A). In contrast, echocardiographic and MRI analysis of four-week mice showed that there was significant chamber dilatation as evidenced by increases in LV end systolic and diastolic volumes, and significant contractile impairment as evidenced by a marked reduction in ejection fraction. There was also evidence of LV posterior wall thinning. Heart rates were similar in the two groups (Fig. 3A, B). In addition increased relaxation time of a gadolinium contrast agent in magnetic resonance imaging (MRI) of hearts suggested functionally relevant fibrotic remodelling of the myocardium (Fig 3C).

Quantitative (q)PCR analysis of csPLA-Tg myocardium showed that there was reduced mRNA expression of *Myh6* and increases in *Myh7*, *Nppa* and *Nppb* mRNA consistent with heart failure (Fig. 4A). This was supported by post-mortem analysis which showed csPLA-Tg hearts were enlarged at four weeks (Fig 4B,C) whilst mass, based on heart weight relative to tibia length, was similar between csPLA-Tg and FLctrl mice at two and four weeks (Fig. 4D). Transudative pleural effusions were evident upon opening the chest cavity in four-week old csPLA-Tg mice symptomatic of heart failure (Fig. 4E).

Enzyme linked immunosorbent assay (ELISA) of blood plasma identified a substantial increase in the plasma concentration of cardiac troponin T in four-week csPLA-Tg mice, indicative of

significant CM damage or death (Fig. 4F). Increases in terminal deoxynucleotidyl transferase dUTP nick end labeling (TUNEL) positive nuclei indicated cell death occurred (Fig. 4G), though there was no evidence of caspase 3 cleavage or lamin cleavage, indicators for apoptosis (Fig. 4H), suggesting necrosis rather than apoptosis was the mode of cell death.

csPLA-Tg myocardium exhibits fibrotic remodelling and an inflammatory senescence associated secretory phenotype

Inspection of Haemotoxylin and Eosin (H&E) stained tissue sections showed that csPLA-Tg heart tissue at two weeks was mostly normal, with sporadic regions of mononuclear aggregation in the myocardial interstitium. At four weeks however csPLA-Tg myocardium was in disarray and substantial mononuclear infiltration was observed (Fig. 5A). Similarly, picrosirius red staining was comparable between csPLA-Tg and FLctrl at two weeks, but at four weeks csPLA-Tg myocardium displayed substantial red staining indicating fibrotic remodelling had occurred (Fig. 5B) supporting the LGE data observed in the MRI assessment of myocardium. Observation of mononuclear infiltration in the myocardium suggested that inflammatory cells were activated and present in csPLA-Tg hearts and this was confirmed by immunofluorescence staining of myocardial sections for CD45 (Fig. 3A), which showed increased numbers of CD45+ cells in the myocardium of both two and four week old mice (Fig. 5C,D). Myocardial inflammation has not previously been reported in models of *LMNA* cardiomyopathy, so to test whether this was unique to our model we performed immunostaining on *Lmna*$^{-/-}$ myocardium for CD45 and observed no increase in CD45+ cells compared with wildtype indicating that this was a feature unique to prelamin A accumulation (Fig. 5E). Furthermore, mRNA expression analysis of myocardium for pro-inflammatory cytokines found that at four weeks *Tnf, Icam1*, *Cxcl1* and *Ccl2* were elevated in csPLA-Tg myocardium (Fig. 5F).

Because disruption to the nuclear lamina is associated with premature senescence (28, 29) and in turn senescence is associated with inflammation via the senescence-associated secretory phenotype (SASP) (30), we postulated that csPLA-Tg myocardium may display traits of senescence. This was supported by q-PCR, which showed expression of mRNA for the genes encoding senescence markers p16 *(Cdkn2a*) and p21 (*Cdkn1a*), were upregulated in four-week csPLA-Tg myocardium (Fig 5F).

Immunohistochemistry for p16 confirmed an increase at the protein level in four week csPLA-Tg myocardium (Fig. 5G). In addition, intense senescence-associated β-galactosidase (SA-β-gal) staining was observed in four-week csPLA-Tg myocardium when compared with FLctrl (Fig 5H).

Nuclear factor kappa-light-chain-enhancer of activated B cells (NF-κB) signalling was activated in csPLA-Tg myocardium

NF-κB is a master regulator of inflammation (31). It is also known that prelamin A can activate NF-κB via persistent DNA damage and a non-canonical signalling pathway involving signalling partners such as IκBα (32). Persistent activation of the DNA damage response is also responsible for activation of senescence in laminopathies (9). Thus, we hypothesised this might be activated in csPLA-Tg mice. The p65 subunit of NF-κB is translocated to the nucleus upon activation so to investigate this we performed quantitative immunofluorescence staining and showed that this was occurring at four weeks (Fig. 6A,B). To substantiate this finding Western blot indicated elevated expression of p65 at four weeks but not two weeks (Fig 6C). We then assessed DNA damage signalling by phosphorylated Histone 2AX (γ-H2AX)—a first responder and activator of DNA damage signalling. We found that γ-H2AX staining as a percentage of total nuclear stain was inconsistent in two week myocardium whilst in four-week csPLA-Tg myocardium there was a trend towards an increase ($P = 0.057$) (Fig. 6D,E). To investigate further we assessed the DNA damage transducer Ataxia Telangiectasia Mutated (ATM), which can activate NF-κB signalling via IκBα. Western blotting of myocardial lysates from four-week old mice showed ATM and IκBα were consistently phosphorylated in csPLA-Tg myocardium (Fig. 6F) Taken together these data infer that activation of inflammatory NF-κB signalling via ATM is a consequence of prelamin A accumulation in heart.

Disruption to the LINC complex and cytoskeleton was preceded by loss of histone marks in csPLA-Tg myocardium

Inconsistencies between the activation of NF-κB and the onset of inflammation encouraged us to explore other pathways consistently affected in two week myocardium. The structural hypothesis of lamin dysfunction argues that nuclear envelope disruption can lead to increased susceptibility to

mechanical stress and structural instability of cells (3). Western blotting of LINC complex proteins and the intermediate filament desmin showed profound changes in expression at four weeks but not at two weeks (Fig 7A). Transmission electron microscopy (TEM) of csPLA-Tg myocardium showed that nuclear morphology defects could be observed at four weeks, though not at two weeks (Fig 7B). Another theory of lamin dysfunction hypothesises that regulation of gene expression is affected by lamina disruption. TEM images showed a loss of chromocentres and heterochromatin bundles which did appear to occur at two weeks in csPLA-Tg myocardium (Fig. 8A). We decided therefore to assess the chromatin changes by investigating methylation of lysine 9 of histone 3 (H3K9me3). We performed and quantified immunohistochemical staining for H3K9me3 expression and discovered a profound loss of H3K9me3 in two week csPLA-Tg myocardium (Fig. 8B)).

Prelamin A accumulates in HIV patients undergoing antiretroviral therapy with protease inhibitors

Because we observed an inflammatory phenotype in the csPLA-Tg model, we postulated this may also occur in the human setting. Due to the paucity of material we were unable to test this with CD45+ staining. However, visualisation of the prelamin A stained tissue sample showed regions containing large clusters of nuclei indicative of leukocyte infiltration, which was not observed to the same extent in non-prelamin A expressing DCM tissue (Fig. 9A). Subsequently we studied the literature for inflammatory cardiomyopathies and focussed on HIV associated cardiomyopathy (33). Because of the association of HIV PIs with the accumulation of prelamin A in other tissues we hypothesised that prelamin A would be abundant in HIV+ patients on a regime of HIV PIs exhibiting symptoms of cardiomyopathy as proven by echocardiographic assessment (Table 1). Histological assessment by H/E and immunohistochemistry for CD3+ and prelamin A confirmed the presence of inflammation in conjunction with prelamin A expression (Fig. 9B). Indeed, prelamin A immunohistochemistry showed focal expression of prelamin A in nuclei of CM and non-CM populations within the hearts of HIV+ patients with a number of CM nuclei showing highly aberrant morphologies. Western blotting also revealed that abundance of prelamin A was increased in HIV+ patients compared to a non-failing control (Fig 9C). Aberrant nuclear morphology and changes in the

spatial organisation of heterochromatin were also observed at the ultrastructural level in HIV+ myocardium compared to NF controls (Fig. 9D) and these observations were consistent with the nuclear morphology defects and loss of heterochromatin bundles observed by TEM in the csPLA-Tg mice (Fig. 7C, 8A).

Inducible expression of prelamin A in adult hearts causes progressive heart dysfunction, inflammation and premature death

To this point, our model has tested constitutive accumulation of prelamin A, mostly relevant to inherited/genetic cardiomyopathies. Because HIV and associated cardiovascular diseases are predominantly acquired later in life, we wanted to mimic this by testing our model using an inducible MerCreMer system in adult mice and tracking disease onset by monitoring mice and performing serial echocardiography (Fig. 10A). We induced mice at 34 ± 3 weeks of age with tamoxifen which led to nuclear envelope accumulation of prelamin A (Fig. 10B). Median survival for csPLA-Tg mice was 65 days post injection (Fig. 10C). Whilst, body weight remained consistent (Fig 10D), ejection fraction was significantly attenuated from 6 weeks onwards and left ventricular end systolic volume was significantly increased at 8 weeks (Fig. 10E). Moreover, histological examination revealed that similar to constitutive expression of prelamin A hearts were fibrotic and subjected to myocardial disarray (Fig 11 A, B). Importantly, CD45+ leukocyte infiltration, indicating inflammation was also evident consistent with the phenotype observed in patients with acquired HIV cardiomyopathy (Fig. 11C, D).

Discussion

Accumulation of prelamin A occurs in genetic and HIV associated cardiomyopathy

To date the role of prelamin A in the setting of cardiomyopathy has been understudied. Here, we investigated a cohort of patient samples, for which the primary diagnosis was idiopathic DCM. We showed consistent prelamin A accumulation in one DCM sample and sporadic accumulation in all other samples, including non-failing controls. Although sequencing of this one sample could not be performed, the consistent detection of prelamin A suggested there may be a genetic basis for the

disease in this patient. Additionally, this accumulation is likely to cause and/or exacerbate cardiomyopathy as evidenced by our study of a novel csPLA-Tg mouse line where severe cardiac dysfunction was observed. We also present compelling evidence showing prelamin A accumulation in HIV associated cardiomyopathy, since all samples tested showed elevated prelamin A abundance, and nuclear morphology defects. A feature of HIV cardiomyopathy is inflammation and consistent with a role for prelamin A in this both constitutive and inducible mouse models of prelamin A accumulation developed extensive myocardial inflammation. In the constitutive model we also observed myocardial senescence and mechanistically, we linked the inflammatory response to modulation of NF-κB signalling, via activation of ATM. However, epigenetic changes may also be more important when considering early initiating mechanisms.

Prelamin A accumulation causes "Inflammageing" of the myocardium in mice

Though inflammation is known to occur during and after ischaemic events and later in heart failure (34) it is less commonly described in the progression to DCM. However, HIV associated cardiomyopathy is strongly associated with an inflammatory response in the myocardium (35, 36). Recent reports show that HAART exposure in perinatal cases of HIV ultimately benefits heart function compared with patients from the pre-HAART era (37) for whom opportunistic infections (38) and potential incorporation and replication of HIV into CMs were problematic (39). Nevertheless, a decline in cardiac function occurs when compared to the normal population and HAART therapies may contribute to this. NRTI's, which prevent replication of HIV, also inhibit transcription of mitochondrial DNA and have been shown to cause cardiac dysfunction in mice (25, 26). Our study presents evidence that inflammation is the key outcome of prelamin A accumulation in CMs, and this is also a relatively unique phenotype of HIV associated cardiomyopathy. Though not subjected to rigorous interrogation of inflammatory pathways, global *Zmpste24*$^{-/-}$ mouse myocardium also showed leukocyte infiltration further supporting a role for prelamin A toxicity in driving inflammation (40). In contrast, inflammation has not been reported in other *Lmna* mouse models of cardiomyopathy. Moreover, cardiomyocyte specific overexpression of wildtype lamin A in mice showed no phenotypic effect or impact on survival implying that processing mechanisms are able to

cope with an increase in prelamin A concentration (41). In this context, it appears that accumulation of prelamin A which cannot be processed, is pathogenic.

We provide evidence that the trigger for inflammation is likely linked to myocardial senescence. Whilst expression of γ-H2AX, the most commonly used marker for DNA damage, was inconsistent in csPLA-Tg myocardium, ataxia telangiectasia mutated (ATM) which signals down-stream of γ-H2AX, was persistently phosphorylated at four weeks. We observed that p16 and p21 mRNA was increased, along with mRNA of pro-inflammatory cytokines Tnf-α, Icam1, Cxcl1, Ccl2, suggesting that myocardium in these mice exhibit the SASP. We were able to further substantiate this by the detection of senescence associated β galactosidase (SA-β-Gal) in csPLA-Tg myocardium. Furthermore, these data concur with previous work showing that when prelamin A accumulates in vascular smooth muscle cells activation of the SASP occurs (42).

Early loss of repressive histone marks indicates gene expression pathways are initiators of pathogenesis

Global *Zmpste24*$^{-/-}$ mice suffer from systemic inflammation arising from non-canonical ATM-dependent NF-κB signalling (32) and we showed that this pathway was activated locally in csPLA-Tg hearts at four-weeks making it likely that increases in SASP factors are caused by activation of NF-κB. However, the absence of NF-κB signalling at two weeks suggests that this inflammatory pathway propagates rather than initiates disease mechanisms. Therefore, we speculated to other mechanisms for disease genesis. One of these was based on the mechanical hypothesis of lamin dysfunction. We reasoned that susceptibility to mechanical stress, which is continual and repetitive in the heart, might lead to structural defects in the nuclear envelope and cytoskeleton. However, in the main these were not observed until four weeks, meaning this was unlikely. *Myh6* and *Myh7* mRNA encoding α- and β-MHC respectively did change at 2 weeks and may indicate early changes to myofilament structure and may also reflect global changes in transcriptional activity as preceding structural defects. Therefore we speculate epigenetic changes may prime the tissue for disease, since chromatin displacement and loss of H3K9me3 were observed in two week mouse hearts. The mechanisms downstream of this remain to be determined but may involve misregulation of the polycomb

repressive complexes (43), known to control senescent genes such as those encoding p16 and p21 and potentially induce SASP independently of DNA damage pathways (44).

Study Limitations

Due to difficulties in obtaining human tissue, we do not have the relevant 'control' groups i.e. HIV PI naïve and/or on alternate therapies i.e. NNRTIs, to fully conclude that HIV PIs are the cause of prelamin A accumulation, though based on current literature it is unlikely that these groups of patients would experience prelamin A accumulation.

Our constitutive mouse model was highly malignant and as such does not perhaps faithfully model the situation in cardiomyopathy, which tends to be more progressive in nature, though the *LMNA* cardiomyopathies are amongst the most severe. However our inducible model was far less severe and represented a more progressive disease and is also relevant to HIV associated cardiomyopathy which are likely to be propagated by the accumulation of prelamin A where HIV PIs with high binding affinity to ZMPSTE24 are still being used for treatment. However one key difference is the model we used relied on mutating the site of ZMPSTE24 cleavage and so does not fully model the problem in HIV associated cardiomyopathy, where a *Zmpste24* Knockout or HIV PI pharmacological intervention would be interesting for further study. However, despite this our study shows in a reductionist manner that prelamin A is a toxic mediator of disease in cardiac tissue indicating that disease is likely to be mediated by the accumulation of prelamin A specifically rather than any divergent targets or pathways such as the declogging of translocons, the only other known and recently discovered function of ZMPSTE24 (45-47).

Conclusions

In summary we have identified a novel role for prelamin A in HIV associated and dilated cardiomyopathies. Accumulation of prelamin A has catastrophic consequences for the integrity of the myocardium resulting in an "inflammageing" phenotype and subsequent loss of contractility. Whilst targeting inflammation potentially via ATM activity may prove useful for patients with established DCM owing to prelamin A accumulation, the immediate translational aspect of this study lies in the

implications for the treatment of HIV associated cardiomyopathy patients, for whom, a change of therapy may have a beneficial outcome in the clinic. Elegant biochemistry performed by Robinson and colleagues provided compelling evidence that HIV PIs bind and block activity of ZMPSTE24 (48). Moreover they were also able to show a rank order of affinity to ZMPSTE24 of HIV PIs currently available for use- lopinavir > ritonavir > amprenavir > darunavir. Of these, darunavir was shown not to bind *ZMPSTE24* at all, which confirms earlier work (49). Many HIV+ patients suffering from cardiac symptoms are not currently using darunavir in their HAART regimes (Table 1). Adjusting HAART regimes to incorporate darunavir and other HIV protease inhibitors with low affinity to ZPMSTE24 may reduce prelamin A accumulation and provide therapeutic benefit for patients suffering from symptoms of HIV associated cardiomyopathy. Moreover, many therapeutic regimes are now beginning to move away from a HIV PI backbone, in favour of non-nucleoside reverse transcriptase inhibitors (NNRTIs) i.e. rilvipirine, and such an approach should be considered in patients with cardiac side-effects who are still receiving high doses of HIV PIs.

Materials and Methods

Generation of cardiomyocyte (CM) specific prelamin A transgenic (csPLA-Tg) mice

This mouse model was commissioned from Taconic-Artemis with the aim to devise a transgenic system to assess the *in vivo* effects of uncleavable prelamin A overexpression. We performed site directed mutagenesis of the human *LMNA* gene at leucine 647 and replaced it with arginine (*LMNA*-L647R). This corresponds to the cleavage site for *ZMPSTE24* and blocks cleavage. The system involved recombinase mediated cassette exchange (RMCE) of the Rosa26 gene whereby *LMNA*-L647R cDNA was inserted into an exchange vector containing a neomycin resistance gene, a strong CAGGS promoter sequence and a STOP cassette flanked by loxP sites. Electroporation into the embryonic stem (ES) cells of C57BL/6 mice led to site-specific recombination by the recombinases F3 and FRT. Neomycin resistant clones that had undergone RMCE were selected. After administration of hormones, superovulated BALB/c females were mated with BALB/c males. Blastocysts were isolated from the uterus at 3.5 days post coitum (dpc) for microinjection. Blastocysts

were placed in a drop of DMEM with 15% FCS under mineral oil. A flat tip, piezo actuated microinjection-pipette with an internal diameter of 12-15 µm was used to inject 10-15 targeted C57BL/6NTac ES cells into each blastocyst. After recovery, 8 injected blastocysts were transferred to each uterine horn of 2.5 dpc, pseudopregnant NMRI females. Chimerism was measured in chimeras (G0) by coat colour contribution of ES cells to the BALB/c host (black/white). Highly chimeric mice were bred to strain C57BL/6 females. Recombination by mating with mice carrying cre-recombinase under the control of the myosin light chain 2 ventricular (MLC2v) promoter led to removal of the stop cassette allowing expression of uncleavable prelamin A in nuclei of CMs of affected offspring. These mice were called CM specific prelamin A transgenic (csPLA-Tg) mice. They were compared to mice expressing the transgene but retaining the lox P sites, termed floxed controls (FLctrl). For investigation of inducible prelamin A expression, breeding was performed with mice expressing cre recombinase flanked by fragments of the estrogen receptor (MerCreMer) which allowed tamoxifen inducible expression also under the control of the MLC2v promoter and were termed *i*nducible-(*i)*csPLA-Tg. Induction was performed by three once-per-day intra-peritoneal injections of 20 mg/kg of Tamoxifen dissolved in peanut oil. Genotyping was performed by PCR on ear tissue DNA using primers designed to detect both the wildtype Rosa26 (377bp) and modified Rosa26 (200bp) loci: Forward 5' GTGGATGCTGAGAACAGGC 3', reverse: 5' TCCACCTGGTCCTCATGC 3' and also for the expression of Cre recombinase: Forward: TGCCAGGATCAGGGTTAA, reverse 5' CCCGGCAAAACAGGTAGTTA 3'. cycling parameters were initial denaturation 95°C 1 min, denaturation 95°C 30 seconds*, annealing 60°C 30 seconds*, extension 72° 1 min*, final extension 72°C 10 min, cooled to 4°C indefinitely. (*repeated for 35 cycles) All csPLA-Tg mice used in the study were heterozygous for the transgene and generated on a C57Bl6 background. Mice were kept in individually ventilated cages (IVC) at the biological services unit (BSU) at the Maurice Wohl Clinical Neuroscience Institute, Kings College London, fed a standard chow diet and kept on a 12 hour light/dark cycle. Male and female mice were used in this study

Lmna$^{-/-}$ mice

A heterozygous breeding colony of mice with a null allele of *Lmna* (50) was established to obtain *Lmna*$^{-/-}$, *Lmna*$^{-/+}$ and *Lmna*$^{+/+}$ (wild-type), Mice were genotyped by PCR on genomic tail DNA using the Manual ArchivePure DNA Purification Kit (5Prime, Gaithersburg, MD, USA) using the following primers: Forward: 5' CGATGAAGAGGGAAAGTTCG 3', Mutant-specific reverse: 5′GCCGAATATCATGGTGGAAA 3', Wild-type-specific reverse: 5′ CCATGGACTGGTCCTGAAGT 3′. Cycling parameters were the same as for csPLA-Tg genotyping. PCR produced a 750 bp amplicon from the mutated allele and a 520 bp amplicon from wild-type. Mice were housed at the BSU at New Hunts House, King's College London, fed a standard chow diet and kept on a 12 hour light/dark cycle.

Murine echocardiography

Echocardiography was performed using a Vevo® 2100 imaging system with a 30 MHz linear transducer specially designed for small animal studies (VisualSonics, USA). Echocardiography was performed with 5% isofluorane fast induction of anaesthesia followed by maintenance of 1-1.5% isoflurane anaesthesia for 4 week old mice and 2.5% isofluorane for 2 week old mice, which was vaporized in 100% oxygen delivered at 1.5-2 liters/min. Heart rate was kept at ~400-450 beats per minute while respiratory rate was ~100 breaths per minute. Body temperature was ~36.5±1°C.

Murine cardiac Magnetic Resonance Imaging (MRI)

Cardiac MRI was performed at the James Black Centre, King's College London on a 7 Tesla (T) horizontal MR scanner (Varian Inc., Palo Alto, CA) with mice in the prone position. The gradient coil had an inner diameter of 12 cm; the gradient strength was 1000 mT/m (100 G/cm), and rise-time was 120 ms. A quadrature transmit/receive coil (RAPID Biomedical GmbH, Germany) with an internal diameter of 39 mm was used. Anesthesia was maintained with 1.5% isoflurane/98.5% oxygen and body temperature was maintained at 37°C using a warm air fan (SA Instruments, Stony Brook, NY). The ECG was monitored by means of two metallic needles placed subcutaneously in the front paws.

A pressure-transducer for respiratory gating was placed on the animal abdomen. To synchronize data acquisition with the ECG and to compensate for respiratory motion, simultaneous ECG triggering and respiration gating (SA Instruments) were applied. Functional and volumetric parameters were achieved following a multi slice Cine-FLASH acquisition (51). These parameters were used: FOV = 25 x 25 mm^2, slide thickness = 1 mm, matrix size = 128 x 128, 9 to 10 frames/cycle, 9 slices, flip angle =40°, cardiac cycle = 120 ± 30 ms, averages = 3, acquisition time ≈ 8 min. Functional and volumetric parameters were calculated from cine-FLASH images and areas of contrast-enhancement were calculated using a semi-automated in-house developed computer software program (King's College London, ClinicalVolumes).

For detection of myocardial 'scarring' by T1 mapping (52), anaesthetised mice were subject to MR imaging before and 25 min after intraperitoneal (i.p.) administration of 0.75 mmol/kg of gadofosveset trisodium (Ablavar®, Lantheus Medical Imaging, North Billerica, MA), a gadolinium-based contrast agent. An ECG triggered, single slice, Look-Locker acquisition was used for T1 mapping and to measure R1 values of the myocardium. The slice was selected in the middle of the heart. Imaging parameters included FOV = 25 x 25 mm^2, slice thickness = 1 mm, matrix size = 128 x 128, 3 phases/cycle, total of 30 phases, 1 slice, flip angle = 10°, TR. 2700 ms, TReff ≈ 40 ms ((cardiac cycle)/(3 phase/cycle)), TE = 2 ms, cardiac cycle = 120 ± 20 ms, number of averages = 1, acquisition time ≈ 13 min. T1-weighted sequences were analysed to assess the R1 values of the myocardium.

Look-Locker T1 mapping resulted in 30 images (3 per cardiac cycle) from which R1 values of blood, infarcted, remote and healthy myocardium were calculated using an exponential 3 parameter fit (A-B*exp (-TI/T1*)) with subsequent T1 correction (OriginLab Corporation, Wellesley, USA).

Transmission Electron Microscopy (TEM)

Mice were injected intraperitoneally with heparin (5000 u/kg body weight). This was followed by intraperitoneal injection of 50mg/kg body weight of sodium pentobarbital to induce terminal anaesthesia. The chest cavity was opened and secured with a hemostat. The LV was injected with a needle connected via a pump to a reservoir of pre-wash buffer. Flow rate of the pump was adjusted as

to perfuse mouse heart at a pressure between 90-100 mmHg with pre-wash buffer. Pre-wash buffer was a standard physiological tyrode solution containing 10mM BDM to arrest the heart in diastole and 2.5% PVP to replace the protein content of blood, thereby maintaining colloidal pressure and preventing haemorrhage at vascular sites in the heart. Following prewash, the hearts were perfused with fixative solution containing 2% Glutaraldehyde and 2% Paraformaldehyde until 20ml of fixative had been perfused. Hearts were dissected and the mid LV was isolated and cut for further processing. Samples were dehydrated through a graded series of ethanol washes and embedded in epoxy resin. Semi-thin sections (0.2 μm) were stained with toluidine blue for light microscopy examinations and were used to guide sampling for TEM studies. Thin sections (0.09 μm) were collected on 150-mesh copper grids and double stained with uranyl acetate and lead citrate for examination under TEM (H7650, Hitachi, Tokyo, Japan).

Human HIV+ samples were fixed in 2% glutaraldehyde in a 0.1 M phosphate buffer, at pH 7.3, post fixed in osmium tetroxide and processed following a standard schedule for embedding in Epon resin. Semi-thin sections were stained either with azur-II or basic fuchsin solutions and mounted with permount medium. Ultrathin sections (70-80) were stained with uranyl acetate and lead hydroxyde. A Jeol 1400 plus TEM was used for observation and photographic analysis.

Human Echocardiography

Echocardiograophy was performed single centre using a Philips epic ultrasound machine. Echocardiographic parameters were determined according to established criteria (53). In particular, ejection fraction was calculated in the apical 4 and 2-chamber views from three separate cardiac cycles using the modified Simpson's method and left ventricular end-diastolic diameter was measured in long-axis and short-axis view.

Statistics

All *in vivo* and *ex vivo* data of csPLA-Tg versus FLctrl mice were analysed using the a two-way analysis of variance without repeated measures with Sidak’s post hoc test for direct comparison of age-matched groups. Student’s unpaired T-test was applied when only four week old mice were

compared. Where unequal variances were observed Welch's correction was applied. For the analyses of body weights over time and serial echocardiography, two-way analysis of variance with repeated measures was selected with Sidak's post hoc test for comparison of groups at specific time points of the series. Kaplan-Meier survival curves were assessed by the log-rank Cox-Mantel test. Values were expressed as means ± the standard deviation (SD). A p value of <0.05 was considered significant. Tests were performed in Excel (Microsoft) or Prism (GraphPad).

Study approval

This study complies with the declaration of Helsinki. Human DCM specimens were obtained from the Sydney Heart Bank (Hospital Research Ethical Committee approval #H03/118; University of Sydney ethical approval #12146) and from Papworth tissue bank in Cambridge, UK and used in accordance with ethical guidelines of King's College London (REC reference 13/LO/1950) and the current UK law. Studies involving HIV associated cardiomyopathy patient endomyocardial biopsies were approved by the Ethics Committee of La Sapienza University Rome, and performed because despite good control of HIV infection patients were experiencing progressive cardiomyopathy. All patients gave informed consent. All animal procedures were performed in accordance with the Guidance on the Operation of the Animals (Scientific Procedures) Act, 1986 (UK Home Office).

Detailed accounts of other methods used in this study can be found in the online supplement to this article.

Author Contributions

DB and CMS conceived and designed the study, and co-wrote the manuscript and supervised the work. DB also conducted experiments and analysed data. AF, RV, CC, MAR performed all studies concerning HIV patients and corresponding samples. RH performed animal husbandry, morphometry and tissue collection. SMA performed Immunohistochemistry and data analysis. GV-B prepared the samples for electron microscopy. AP performed and analysed the murine cMRI. PSZ supplied the *Lmna*$^{-/-}$ mice. EE and CdR sourced and supplied the DCM explants and Non-failing Donor heart tissue. AMS co-supervised the study and contributed to manuscript preparation.

Acknowledgments

We would like to acknowledge and thank the Papworth Hospital Research Tissue Bank (Cambridge, UK) for providing additional explanted DCM samples.

Sources of Funding

This study was funded by the British Heart Foundation grant number [PG/15/93/31834]. This study was also supported by AIFA project titled 'Multicenterandomized study on the efficacy of immunosuppression in patients with virus-negative inflammatory cardiomyopathy' and International research collaboration in the ERA-CVD joint project titled: "Gene profiling test for identification of treatable patients with acute and chronic heart failure (GENPROVIC)". AMS is supported by the BHF (CH/1999001/11735).

Disclosures

None to declare

References

1. van Berlo JH, de Voogt WG, van der Kooi AJ, van Tintelen JP, Bonne G, Yaou RB, et al. Meta-analysis of clinical characteristics of 299 carriers of LMNA gene mutations: do lamin A/C mutations portend a high risk of sudden death? *J Mol Med (Berl).* 2005;83(1):79-83.
2. Fatkin D, MacRae C, Sasaki T, Wolff MR, Porcu M, Frenneaux M, et al. Missense mutations in the rod domain of the lamin A/C gene as causes of dilated cardiomyopathy and conduction-system disease. *The New England journal of medicine.* 1999;341(23):1715-24.
3. Brayson D, and Shanahan CM. Current insights into LMNA cardiomyopathies: Existing models and missing LINCs. *Nucleus.* 2017;8(1):17-33.
4. Andre P, Schneebeli S, Vigouroux C, Lascols O, Schaaf M, and Chevalier P. Metabolic and cardiac phenotype characterization in 37 atypical Dunnigan patients with nonfarnesylated mutated prelamin A. *Am Heart J.* 2015;169(4):587-93.
5. Brodsky GL, Bowersox JA, Fitzgerald-Miller L, Miller LA, and Maclean KN. The prelamin A pre-peptide induces cardiac and skeletal myoblast differentiation. *Biochem Biophys Res Commun.* 2007;356(4):872-9.
6. Galant D, Gaborit B, Desgrouas C, Abdesselam I, Bernard M, Levy N, et al. A Heterozygous ZMPSTE24 Mutation Associated with Severe Metabolic Syndrome, Ectopic Fat Accumulation, and Dilated Cardiomyopathy. *Cells.* 2016;5(2).
7. Taylor MR, Fain PR, Sinagra G, Robinson ML, Robertson AD, Carniel E, et al. Natural history of dilated cardiomyopathy due to lamin A/C gene mutations. *J Am Coll Cardiol.* 2003;41(5):771-80.

8. Ben-Harush K, Wiesel N, Frenkiel-Krispin D, Moeller D, Soreq E, Aebi U, et al. The supramolecular organization of the C. elegans nuclear lamin filament. *J Mol Biol.* 2009;386(5):1392-402.
9. Liu B, Wang J, Chan KM, Tjia WM, Deng W, Guan X, et al. Genomic instability in laminopathy-based premature aging. *Nat Med.* 2005;11(7):780-5.
10. Misteli T, and Scaffidi P. Genome instability in progeria: when repair gets old. *Nat Med.* 2005;11(7):718-9.
11. Isermann P, and Lammerding J. Nuclear mechanics and mechanotransduction in health and disease. *Current biology : CB.* 2013;23(24):R1113-21.
12. Davies BS, Fong LG, Yang SH, Coffinier C, and Young SG. The posttranslational processing of prelamin A and disease. *Annu Rev Genomics Hum Genet.* 2009;10:153-74.
13. Beck LA, Hosick TJ, and Sinensky M. Isoprenylation is required for the processing of the lamin A precursor. *The Journal of cell biology.* 1990;110(5):1489-99.
14. Sinensky M. Recent advances in the study of prenylated proteins. *Biochimica et biophysica acta.* 2000;1484(2-3):93-106.
15. Sinensky M, Fantle K, Trujillo M, McLain T, Kupfer A, and Dalton M. The processing pathway of prelamin A. *J Cell Sci.* 1994;107 (Pt 1):61-7.
16. Weber K, Plessmann U, and Traub P. Maturation of nuclear lamin A involves a specific carboxy-terminal trimming, which removes the polyisoprenylation site from the precursor; implications for the structure of the nuclear lamina. *FEBS letters.* 1989;257(2):411-4.
17. Gerhard-Herman M, Smoot LB, Wake N, Kieran MW, Kleinman ME, Miller DT, et al. Mechanisms of premature vascular aging in children with Hutchinson-Gilford progeria syndrome. *Hypertension.* 2012;59(1):92-7.
18. Olive M, Harten I, Mitchell R, Beers JK, Djabali K, Cao K, et al. Cardiovascular pathology in Hutchinson-Gilford progeria: correlation with the vascular pathology of aging. *Arterioscler Thromb Vasc Biol.* 2010;30(11):2301-9.
19. Prakash A, Gordon LB, Kleinman ME, Gurary EB, Massaro J, D'Agostino R, Sr., et al. Cardiac Abnormalities in Patients With Hutchinson-Gilford Progeria Syndrome. *JAMA Cardiol.* 2018;3(4):326-34.
20. Coffinier C, Hudon SE, Farber EA, Chang SY, Hrycyna CA, Young SG, et al. HIV protease inhibitors block the zinc metalloproteinase ZMPSTE24 and lead to an accumulation of prelamin A in cells. *Proc Natl Acad Sci U S A.* 2007;104(33):13432-7.
21. Laurence J, Elhadad S, Robison T, Terry H, Varshney R, Woolington S, et al. HIV protease inhibitor-induced cardiac dysfunction and fibrosis is mediated by platelet-derived TGF-beta1 and can be suppressed by exogenous carbon monoxide. *PLoS One.* 2017;12(10):e0187185.
22. Shah ASV, Stelzle D, Lee KK, Beck EJ, Alam S, Clifford S, et al. Global Burden of Atherosclerotic Cardiovascular Disease in People Living with the Human Immunodeficiency Virus: A Systematic Review and Meta-Analysis. *Circulation.* 2018.
23. Frustaci A, Petrosillo N, Francone M, Verardo R, Ippolito G, and Chimenti C. Biopsy-proven autoimmune myocarditis in HIV-associated dilated cardiomyopathy. *BMC Infect Dis.* 2014;14:729.
24. Lumsden RH, and Bloomfield GS. The Causes of HIV-Associated Cardiomyopathy: A Tale of Two Worlds. *Biomed Res Int.* 2016;2016:8196560.
25. Lewis W, Grupp IL, Grupp G, Hoit B, Morris R, Samarel AM, et al. Cardiac dysfunction occurs in the HIV-1 transgenic mouse treated with zidovudine. *Lab Invest.* 2000;80(2):187-97.
26. Lewis W, Simpson JF, and Meyer RR. Cardiac mitochondrial DNA polymerase-gamma is inhibited competitively and noncompetitively by phosphorylated zidovudine. *Circ Res.* 1994;74(2):344-8.
27. Butler J, Kalogeropoulos AP, Anstrom KJ, Hsue PY, Kim RJ, Scherzer R, et al. Diastolic Dysfunction in Individuals With Human Immunodeficiency Virus Infection: Literature Review,

Rationale and Design of the Characterizing Heart Function on Antiretroviral Therapy (CHART) Study. *J Card Fail.* 2018;24(4):255-65.
28. Bonello-Palot N, Simoncini S, Robert S, Bourgeois P, Sabatier F, Levy N, et al. Prelamin A accumulation in endothelial cells induces premature senescence and functional impairment. *Atherosclerosis.* 2014;237(1):45-52.
29. Ragnauth CD, Warren DT, Liu Y, McNair R, Tajsic T, Figg N, et al. Prelamin A acts to accelerate smooth muscle cell senescence and is a novel biomarker of human vascular aging. *Circulation.* 2010;121(20):2200-10.
30. Tchkonia T, Zhu Y, van Deursen J, Campisi J, and Kirkland JL. Cellular senescence and the senescent secretory phenotype: therapeutic opportunities. *J Clin Invest.* 2013;123(3):966-72.
31. Valen G, Yan ZQ, and Hansson GK. Nuclear factor kappa-B and the heart. *J Am Coll Cardiol.* 2001;38(2):307-14.
32. Osorio FG, Barcena C, Soria-Valles C, Ramsay AJ, de Carlos F, Cobo J, et al. Nuclear lamina defects cause ATM-dependent NF-kappaB activation and link accelerated aging to a systemic inflammatory response. *Genes Dev.* 2012;26(20):2311-24.
33. Trachtenberg BH, and Hare JM. Inflammatory Cardiomyopathic Syndromes. *Circ Res.* 2017;121(7):803-18.
34. Mann DL. Inflammatory mediators and the failing heart: past, present, and the foreseeable future. *Circ Res.* 2002;91(11):988-98.
35. Ntusi N, O'Dwyer E, Dorrell L, Wainwright E, Piechnik S, Clutton G, et al. HIV-1-Related Cardiovascular Disease Is Associated With Chronic Inflammation, Frequent Pericardial Effusions, and Probable Myocardial Edema. *Circ Cardiovasc Imaging.* 2016;9(3):e004430.
36. Ntusi NAB. HIV and myocarditis. *Curr Opin HIV AIDS.* 2017;12(6):561-5.
37. Lipshultz SE, Wilkinson JD, Thompson B, Cheng I, Briston DA, Shearer WT, et al. Cardiac Effects of Highly Active Antiretroviral Therapy in Perinatally HIV-Infected Children: The CHAART-2 Study. *J Am Coll Cardiol.* 2017;70(18):2240-7.
38. Anderson DW, and Virmani R. Emerging patterns of heart disease in human immunodeficiency virus infection. *Hum Pathol.* 1990;21(3):253-9.
39. Fiala M, Popik W, Qiao JH, Lossinsky AS, Alce T, Tran K, et al. HIV-1 induces cardiomyopathyby cardiomyocyte invasion and gp120, Tat, and cytokine apoptotic signaling. *Cardiovasc Toxicol.* 2004;4(2):97-107.
40. Pendas AM, Zhou Z, Cadinanos J, Freije JM, Wang J, Hultenby K, et al. Defective prelamin A processing and muscular and adipocyte alterations in Zmpste24 metalloproteinase-deficient mice. *Nat Genet.* 2002;31(1):94-9.
41. Wang Y, Herron AJ, and Worman HJ. Pathology and nuclear abnormalities in hearts of transgenic mice expressing M371K lamin A encoded by an LMNA mutation causing Emery-Dreifuss muscular dystrophy. *Hum Mol Genet.* 2006;15(16):2479-89.
42. Liu Y, Drozdov I, Shroff R, Beltran LE, and Shanahan CM. Prelamin A accelerates vascular calcification via activation of the DNA damage response and senescence-associated secretory phenotype in vascular smooth muscle cells. *Circ Res.* 2013;112(10):e99-109.
43. Boros J, Arnoult N, Stroobant V, Collet JF, and Decottignies A. Polycomb repressive complex 2 and H3K27me3 cooperate with H3K9 methylation to maintain heterochromatin protein 1alpha at chromatin. *Mol Cell Biol.* 2014;34(19):3662-74.
44. Ito T, Teo YV, Evans SA, Neretti N, and Sedivy JM. Regulation of Cellular Senescence by Polycomb Chromatin Modifiers through Distinct DNA Damage- and Histone Methylation-Dependent Pathways. *Cell Rep.* 2018;22(13):3480-92.
45. Ast T, Michaelis S, and Schuldiner M. The Protease Ste24 Clears Clogged Translocons. *Cell.* 2016;164(1-2):103-14.
46. Kayatekin C, Amasino A, Gaglia G, Flannick J, Bonner JM, Fanning S, et al. Translocon Declogger Ste24 Protects against IAPP Oligomer-Induced Proteotoxicity. *Cell.* 2018;173(1):62-73 e9.

47. Spear ED, Hsu ET, Nie L, Carpenter EP, Hrycyna CA, and Michaelis S. ZMPSTE24 missense mutations that cause progeroid diseases decrease prelamin A cleavage activity and/or protein stability. *Dis Model Mech.* 2018;11(7).
48. Mehmood S, Marcoux J, Gault J, Quigley A, Michaelis S, Young SG, et al. Mass spectrometry captures off-target drug binding and provides mechanistic insights into the human metalloprotease ZMPSTE24. *Nat Chem.* 2016;8(12):1152-8.
49. Coffinier C, Hudon SE, Lee R, Farber EA, Nobumori C, Miner JH, et al. A potent HIV protease inhibitor, darunavir, does not inhibit ZMPSTE24 or lead to an accumulation of farnesyl-prelamin A in cells. *J Biol Chem.* 2008;283(15):9797-804.
50. Sullivan T, Escalante-Alcalde D, Bhatt H, Anver M, Bhat N, Nagashima K, et al. Loss of A-type lamin expression compromises nuclear envelope integrity leading to muscular dystrophy. *The Journal of cell biology.* 1999;147(5):913-20.
51. Protti A, Sirker A, Shah AM, and Botnar R. Late gadolinium enhancement of acute myocardial infarction in mice at 7T: cine-FLASH versus inversion recovery. *J Magn Reson Imaging.* 2010;32(4):878-86.
52. Lavin B, Protti A, Lorrio S, Dong X, Phinikaridou A, Botnar RM, et al. MRI with gadofosveset: A potential marker for permeability in myocardial infarction. *Atherosclerosis.* 2018;275:400-8.
53. Quinones MA, Gaasch WH, and Alexander JK. Echocardiographic assessment of left ventricular function with special reference to normalized velocities. *Circulation.* 1974;50(1):42-51.

Tables

Table 1. Clinical characteristics and antiretroviral treatment regime of five patients with HIV-associated cardiomyopathy

HIV+ Patient ID	Age	Sex	Time under retroviral therapy, years	Echocardiography Data	
				LVEDD*, mm	LVEF†, %
Pt1	35	M	10‡	65	29
Pt2	56	M	8§	56	40
Pt3	52	M	9‖	48	43
Pt4	45	M	8#	62	38
Pt5	45	F	9**	68	35
Normal Values				<56	≥50

* LVEDD=Left ventricular end-diastolic diameter

† LVEF= Left ventricular ejection fraction

‡= Emcitrabine/Tenofovir, Atazanavir, Ritonavir,

§=Emcitrabine/Tenofovir, Lopinavir/Ritonavir, Rivotril

‖= Atazanavir, Norvir, Abacavir/Lamivudin

#= Abacavir/Lamivudine, Efavirenz, Atazanavir

** Ritonavir, Rivotril, Lamivudine, Zidovudine, Fosamprenavir

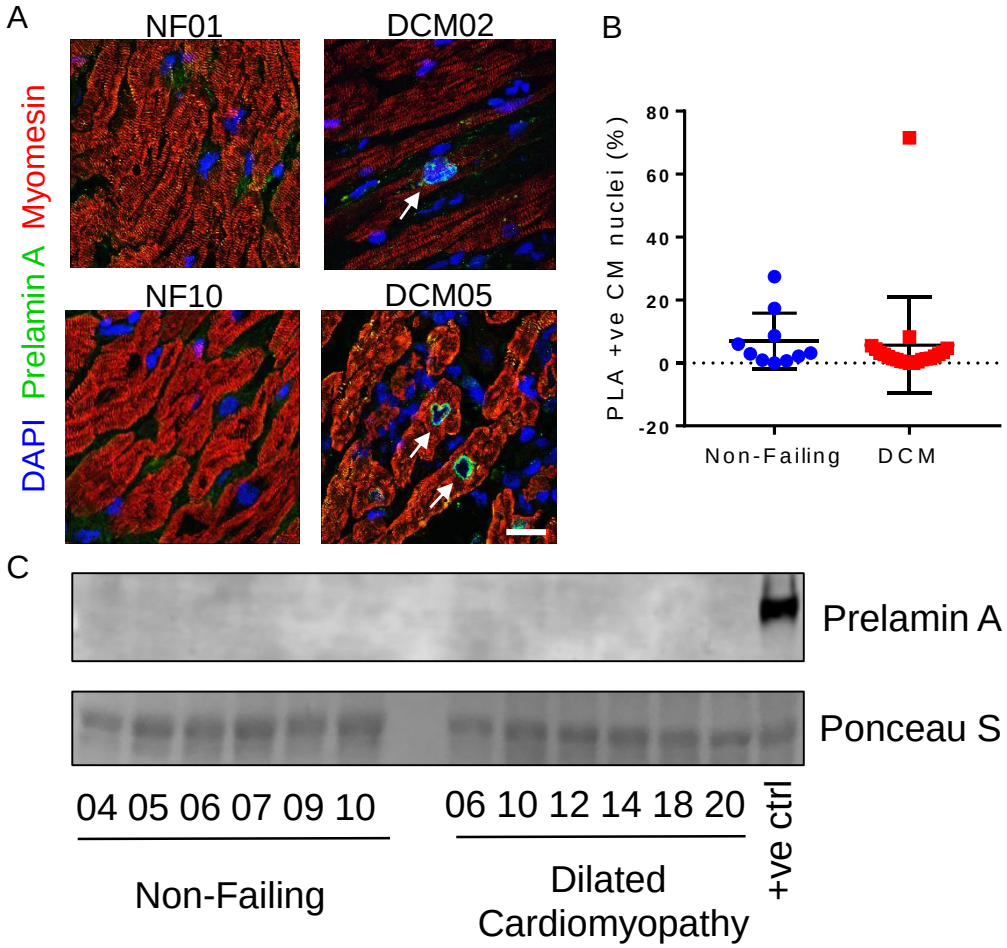

Figure 1. Prelamin A accumulated in a heart of a patient with Dilated Cardiomyopathy. (DCM). A. Confocal micrographs of human heart sections from DCM patients and non-failing (NF) controls subjected to immunofluorescence staining to detect prelamin A (green), myomesin (red) and DAPI (blue). Arrows point to prelamin A positive CM nuclei, many of which exhibit nuclear morphology defects. **B.** the number of nuclei which stained positively for prelamin A were quantified as a percentage of CM nuclei for non-failing (blue circles, N=10 non-failing donor samples) and DCM (red squares, N=21 samples from explanted DCM hearts) myocardial sections (means ± SDs). Scale = 10 μm. **C.** Western blotting did not detect prelamin A in a selection of DCM patient samples. There was not enough sample remaining from DCM05 to run on a western blot.

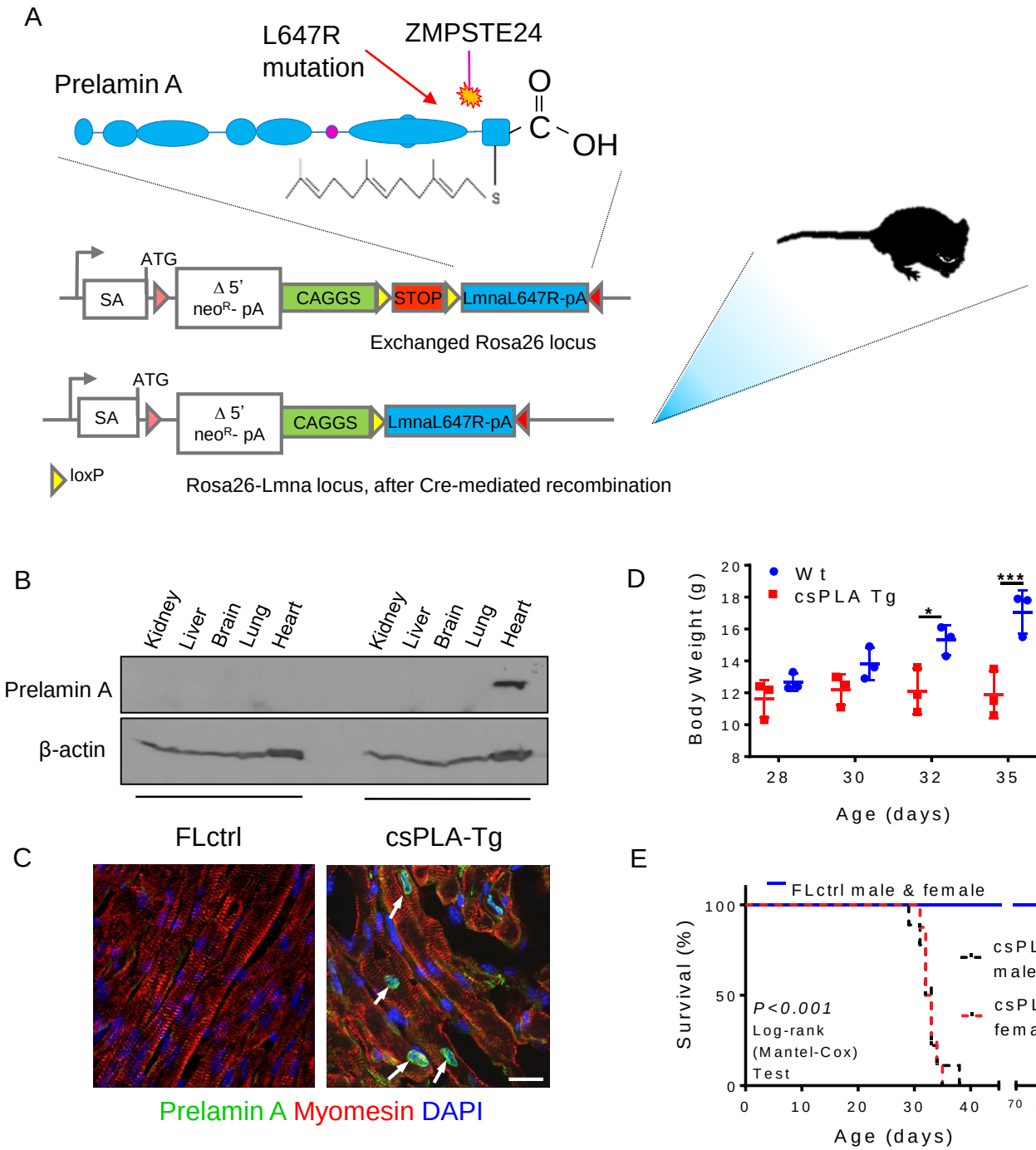

Figure 2. Targeted transgenesis of prelamin A led to nuclear accumulation in CMs and resulted in premature death in mice. A. Schematic representation showing the site of prelamin A (*LMNA*-L647R) cDNA insertion and the modifications required for conditional expression. B. Western blotting for prelamin A showing expression was restricted to heart tissue **C.** Confocal micrographs of myocardium stained for prelamin A showing nuclear rim localisation in csPLA-Tg hearts. Scale = 10 μm. **C.** Growth curves showing that csPLA-Tg mice stop growing after 30 days. N= 3 males/group. Two-way ANOVA with repeated measures with Sidak's post-hoc test for multiple comparisons was perfoprmed. *P<0.05, ***P<0.001. **D.** Kaplan-Meier survival analysis showing that csPLA-Tg male and female mice exhibited attenuated survival compared to FLctrl counterparts. N= 7 FLctrl males, 8 FLctrl females, 9 csPLA-Tg males, 8 csPLA-Tg females. Log-rank Mantel-Cox test was performed. P<0.0001

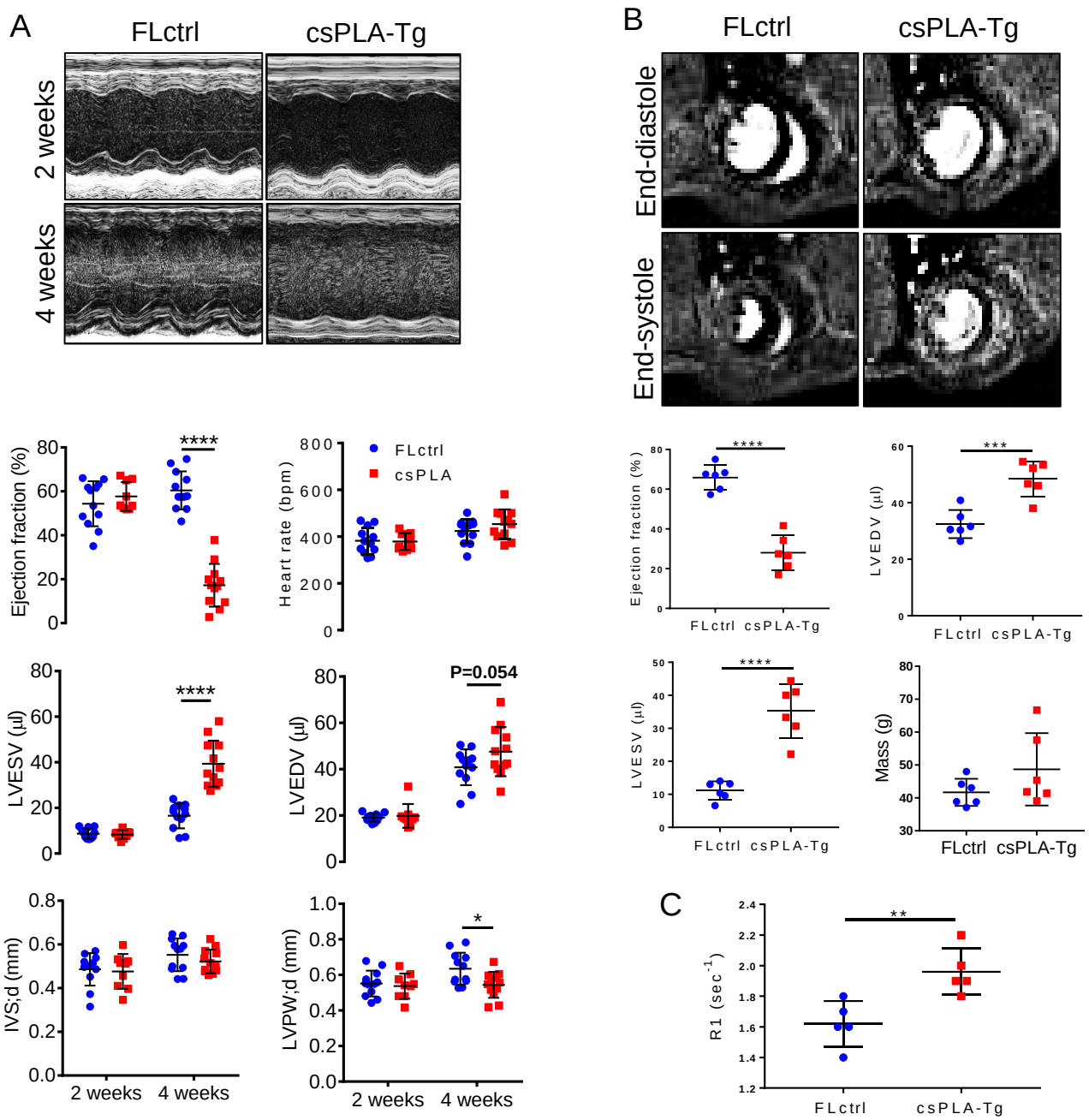

Figure 3. Cardiac function was attenuated in four week old csPLA-Tg mice. A. Representative images of echocardiographs and corresponding graphs of analysis performed on movies acquired in B-mode showing severely compromised cardiac function in four-week old mice N=12/group (6 females, 6 males) except csPLA-Tg 2 weeks which was N= 9 (7 females, 2 males). Values are means ± SDs, Two way ANVOA no repeated measures was performed with Sidak's post hoc test for multiple comparisons. *P<0.05, ***P<0.001, ****P<0.0001 **B.** Representative cardiac MRI images of myocardium in end systole and end diastole and corresponding graphs displaying a decrease in ejection fraction alongside increases in left ventricle end diastolic (LVEDV) and systolic volume (LVESV). Mass was statistically unchanged but with increased variation and concurs with post-mortem heart weight measurements. **C.** Increased relaxation time (R1) of gadolinium contrast in four week csPLA-Tg myocardium indicative of fibrosis remodelling. N= 6 males/group. Values are means ± SDs, Students two-tailed T-test was performed. **P<0.01, ***P<0.001, ****P<0.0001. IVS;d = Intraventricular septal thickness in diastole, LVPW;d = Left ventricle posterior wall thickness in diastole.

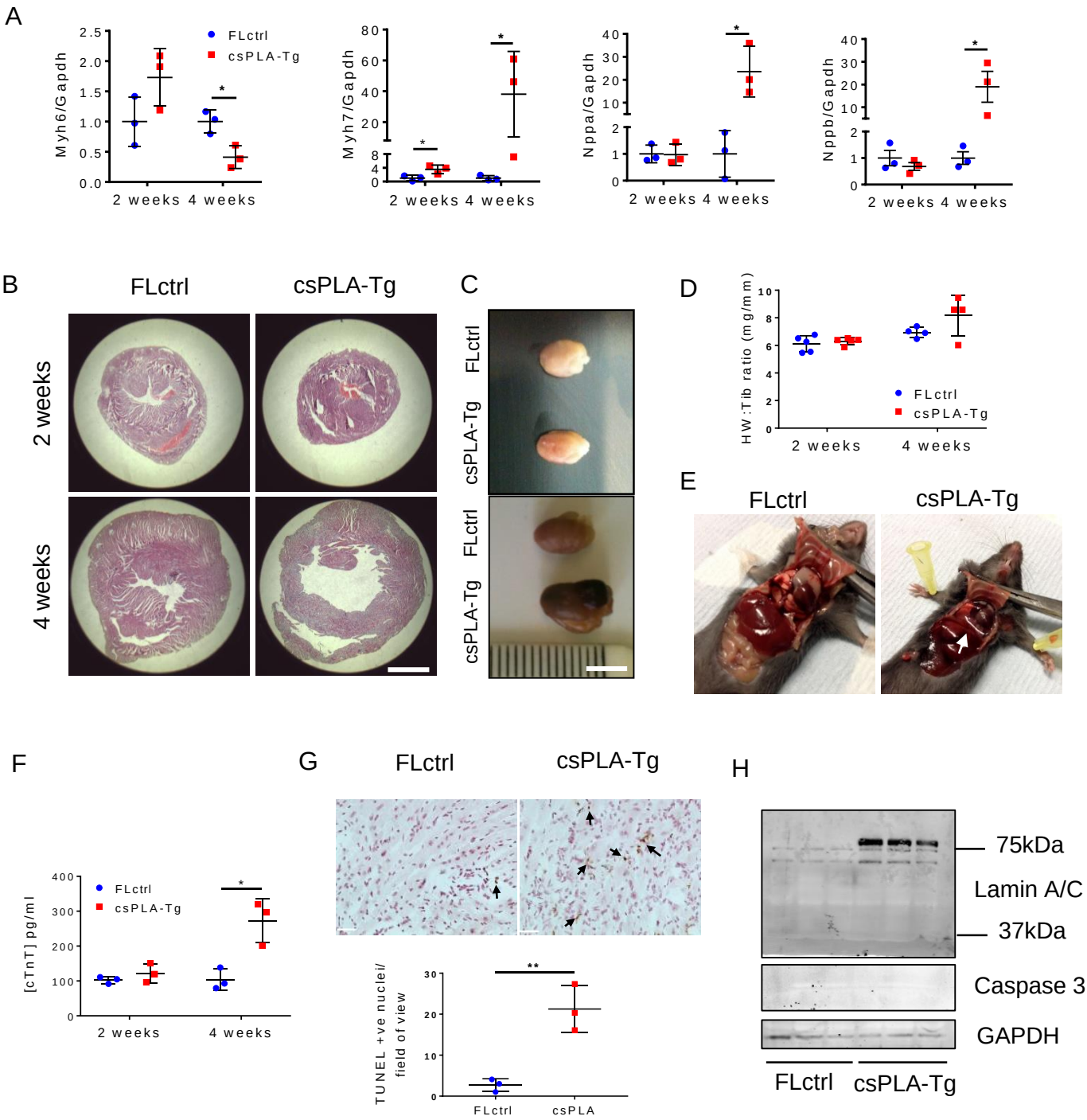

Figure 4. csPLA-Tg mice displayed signs of heart failure and necrotic cell death **A.** Foetal gene expression is dysregulated in csPLA-Tg hearts at four weeks indicating heart failure N=3 females/group. Values are means ± SDs. Two-Way ANVOA no repeated measures was performed with Sidak's post hoc Test for multiple comparisons, *P<0.05. **B.** low magnification micrographs showing cross-sectional view of the heart stained with H&E showing four-week csPLA-Tg mice possessed dilated cardiac chambers. Scale = 2 mm. **C.** Photographs showing csPLA-Tg appeared enlarged at four weeks. Scale = 5mm**. D**. No significant difference in heart weight to tibia length ratio was observed. Values are means ± SDs. N=3/group. **E.** Dissection of chest cavities showing transudative pleural effusions in csPLA-Tg mice. **F.** Blood plasma subjected to ELISA showed elevated levels of circulating cardiac TNT indicative of cardiac damage in four week old mice. N= 3 females/group. Values are means ± SDs. Two-Way ANOVA no repeated measures with Sidak's post hoc test for multiple comparisons was performed. *P<0.05 **G.** TUNEL staining was performed on four week csPLA-Tg heart sections and image quantification showed a significant increase in TUNEL positive nuclei in csPLA-Tg heart sections at four weeks. N= 3 females/group. Values are means ± SDs. Student's two-tailed T-test was perfromed. **P<0.01. **H.** Western blotting showed that cleavage of caspase 3 and lamins A/C, which occurs at ~37 kDa, which occur during apoptosis, did not occur in four week csPLA-Tg myocardium.

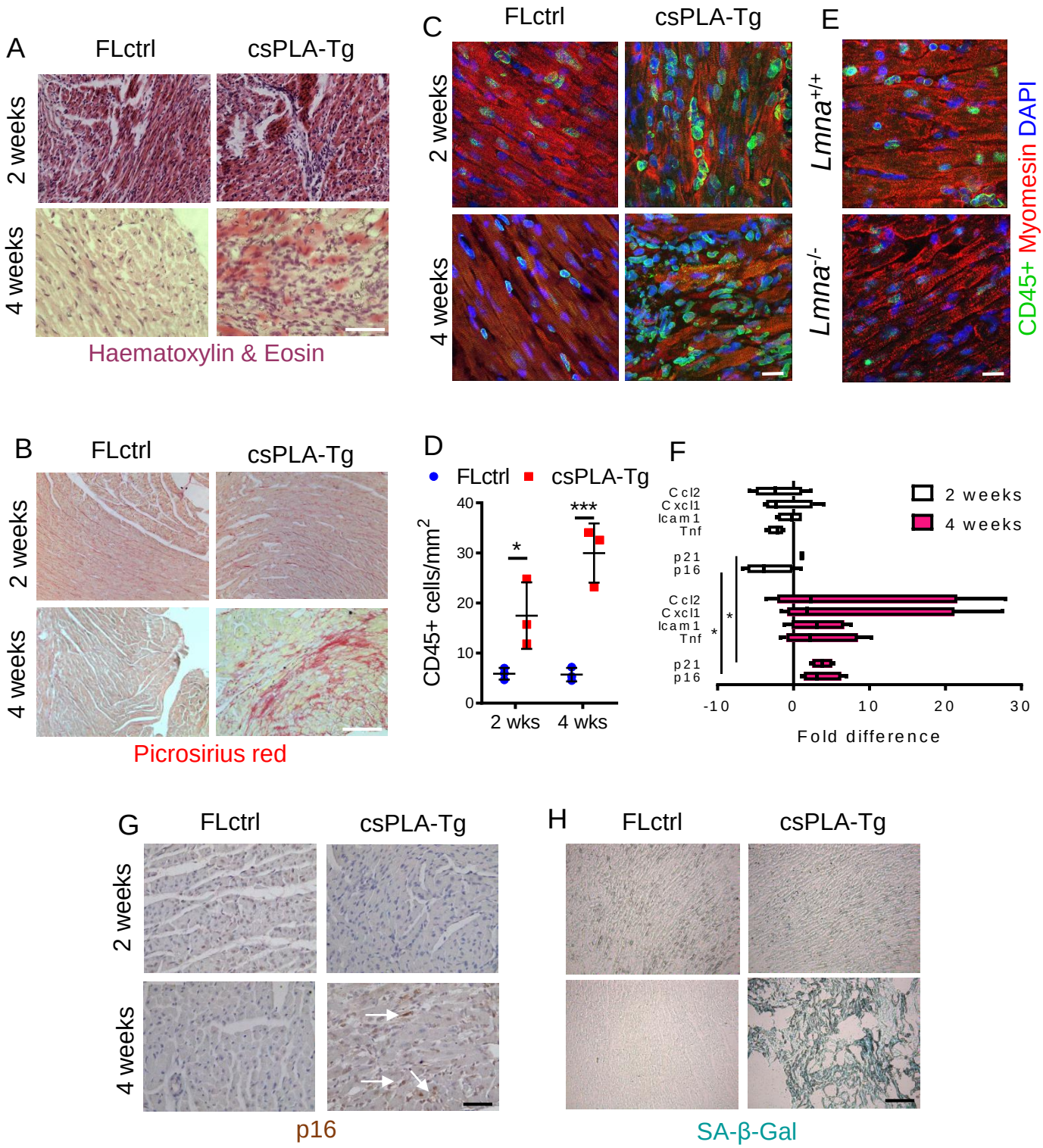

Figure 5. Fibrotic remodelling of csPLA-Tg myocardium occurred in tandem with inflammation and senescence A. Light micrographs showing myocardial disarray in four week csPLA-Tg myocardium stained with Haematoxylin and Eosin. Scale = 30μm. **B.** Light micrographs showing Picrosirius red stained myocardium to indicate fibrosis in four week csPLA-Tg myocardium shown by excessive red staining. Scale = 30μm. **C & D.** Quantitative fluorescence immunostaining for CD45 shows presence of CD45+ cells in two and four-week csPLA-Tg myocardium. Scale = 10 μm. Values are means ± SDs. N=3 females/group. Two-way ANOVA with Sidak's post hoc test for multiple comparisons was performed. **P<0.01 **E.** CD45+ immunostaining of *Lmna*$^{-/-}$myocardium showed no evidence of infiltration by CD45+ leukocyte populations. **F.** qPCR showing the cytokine profile of csPLA-Tg myocardial mRNA. N=4 females/group. **G.** Immunohistochemical staining showing expression of p16 in four week csPLA-Tg myocardium. **H.** Senescence associated β galactosidase was expressed in four week csPLA-Tg myocardium.

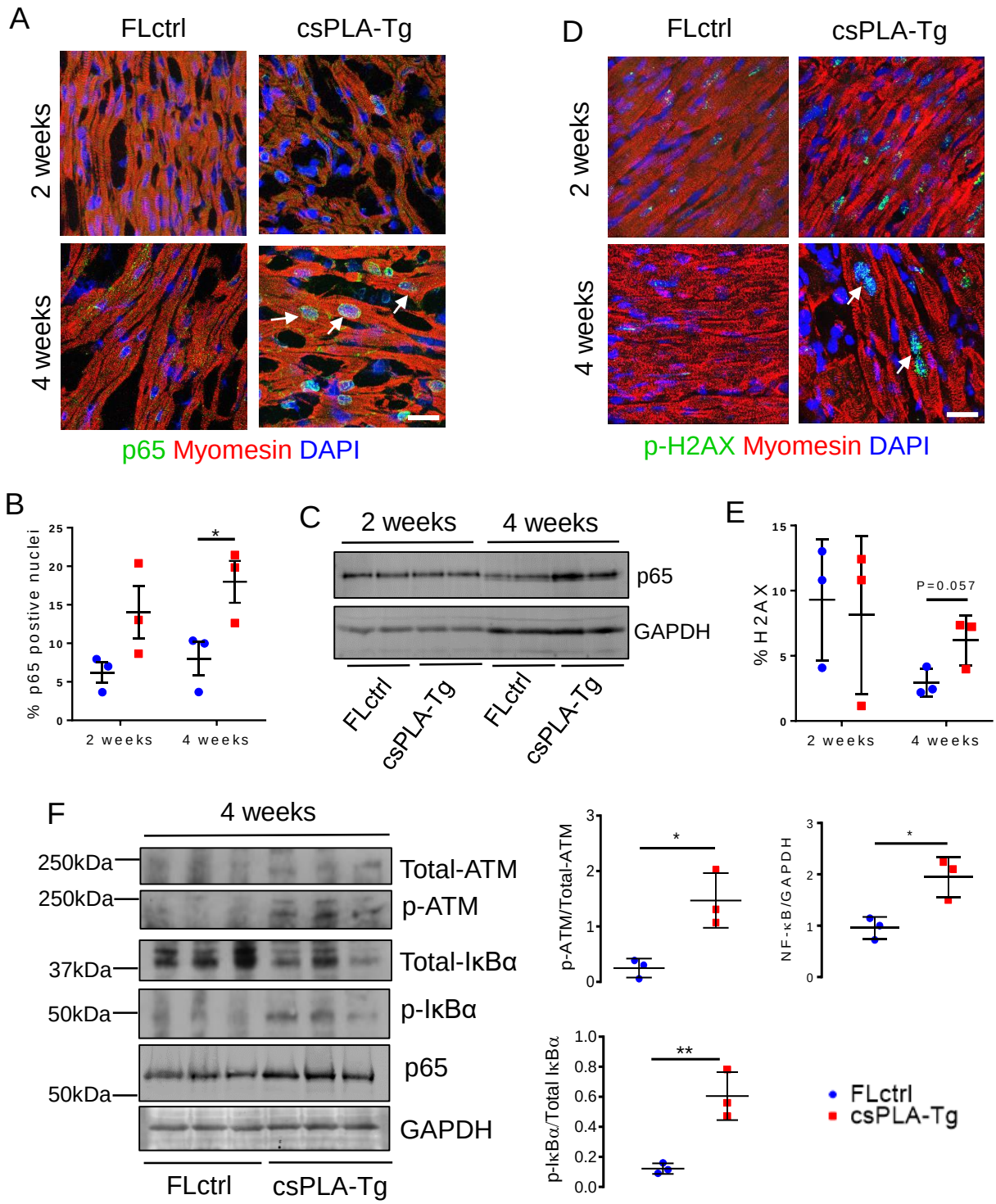

Figure 6. NF-κB signalling was activated in four week csPLA-Tg CMs and mediated by persistent DNA damage. A. Subcellular localisation of p65 subunit of NF-κB in csPLA-Tg myocardium, highlighted by white arrows **B.** quantification of p65 micrographs showing increases in the number of nuclei expressing p65 for two- and four-week hearts counted as a percentage of total nuclei. N=3 females/group. Values are means ± SDs, Two-way ANOVA no repeated measures with Sidak's test for multiple comparisons was performed **C.** Western blot showing increase of NF-κB sub-unit p65 in four week csPLA-Tg myocardium. **D.** Confocal micrographs of fluorescence immunostaining showing DNA damage marker γ-H2AX (white arrows). **E.** Quantification of γ-H2AX micrographs. N=3 females/group. Values are means ± SDs, Two-way ANOVA no repeated measures with Sidak's post hoc test for multiple comparisons was performed. **D.** Western blots of four week myocardial lysates showing phosphorylation status of ATM and IκBα and **E.** graphs showing corresponding densitometry analyses. Scale = 10 μm. Values are means ± SDs. N=3 females/group. Unpaired two-tailed T-test was performed. *P<0.05 **P<0.001.

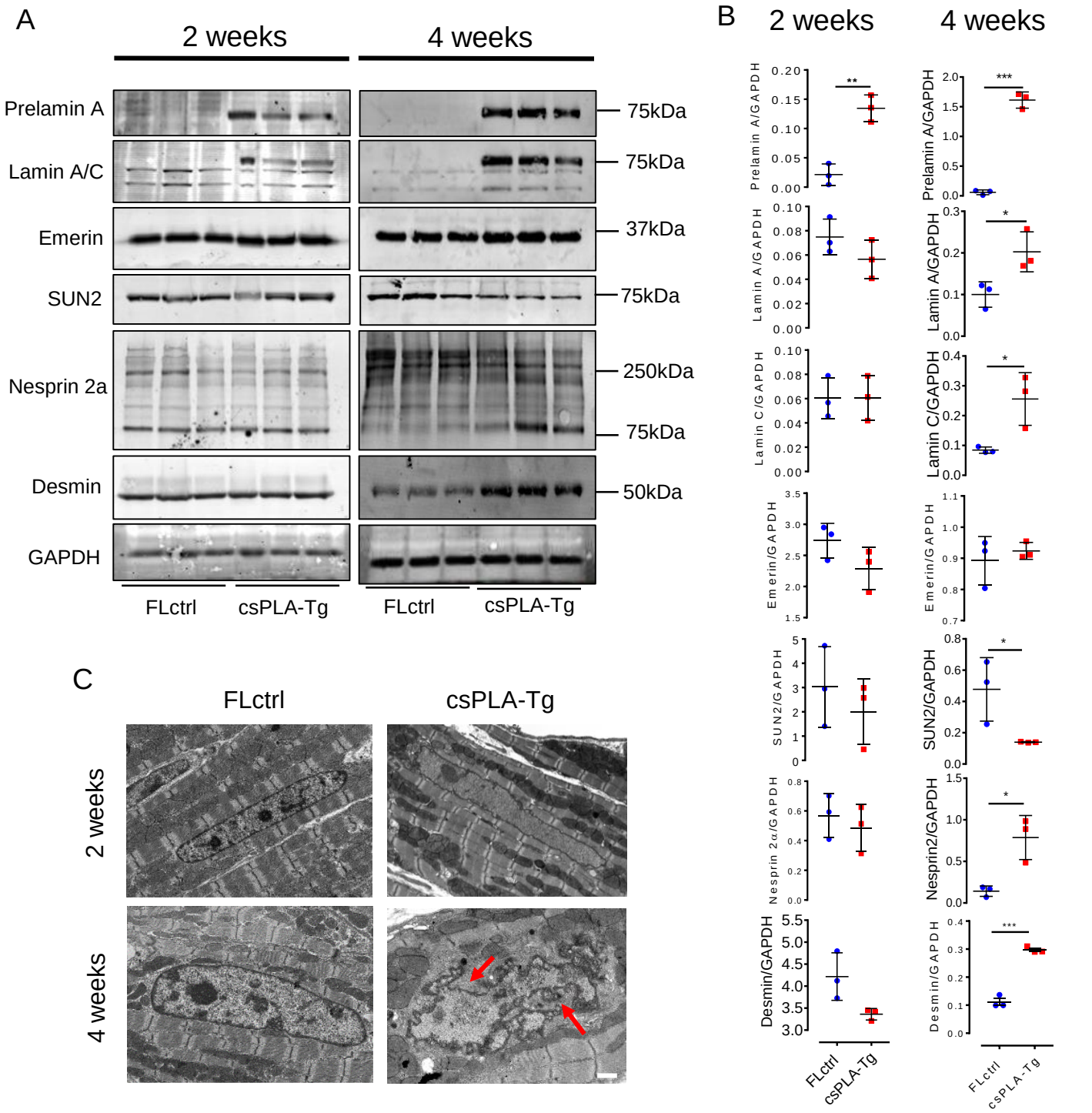

Figure 7. Prelamin A accumulation led to disorganisation of molecular structure at four weeks and loss of chromatin and histone marks at two weeks. A & B. Western blot analysis showing the protein expression changes occurring at four weeks in structural proteins of the nuclear envelope-lamin A/C, emerin, SUN2, nesprin 2, and also the cytoskeleton-desmin, with corresponding semi-quantitative densitometry analysis. N=3 females/group. Values are means ± SDs. Unpaired two tailed T-test was performed on age-matched groups. Welch's correction was applied to data for lamin A, lamin C, emerin, SUN2 and nesprin2 at four weeks. *P<0.05 **P<0.01 ***P<0.001. **C.** Electron micrographs showing nuclear shape and size changes in csPLA-Tg myocardium, red arrows point to regions of nuclear in-folding characteristic of nuclear morphology defects. Scale = 1 µm.

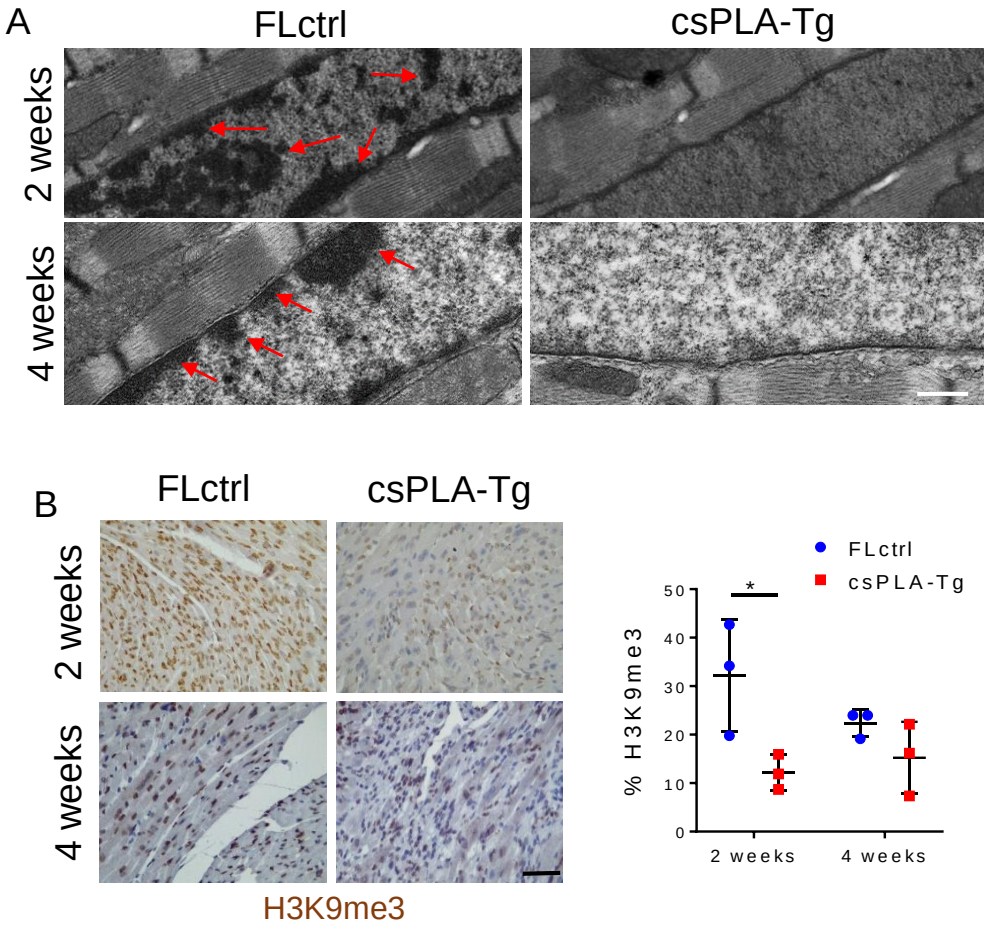

Figure 8. Prelamin A accumulation resulted in loss of heterochromatin and H3K9me3 repressive histone marks in the myocardium of 2 week old mice A. Representative electron micrographs show heterochromatin displacement and loss of chromocentres. Scale = 500 nm. **B.** Quantitative immunohistochemistry showed a profound loss of H3K9me3 staining as a percentage of total Haemotoxylin stain in two week csPLA myocardium. Scale = 30 μm. Values are mean ± SD. N=3 females/group. Two-way ANOVA no repeated measures with Sidak's test for multiple comparisons was performed.* $P<0.05$.

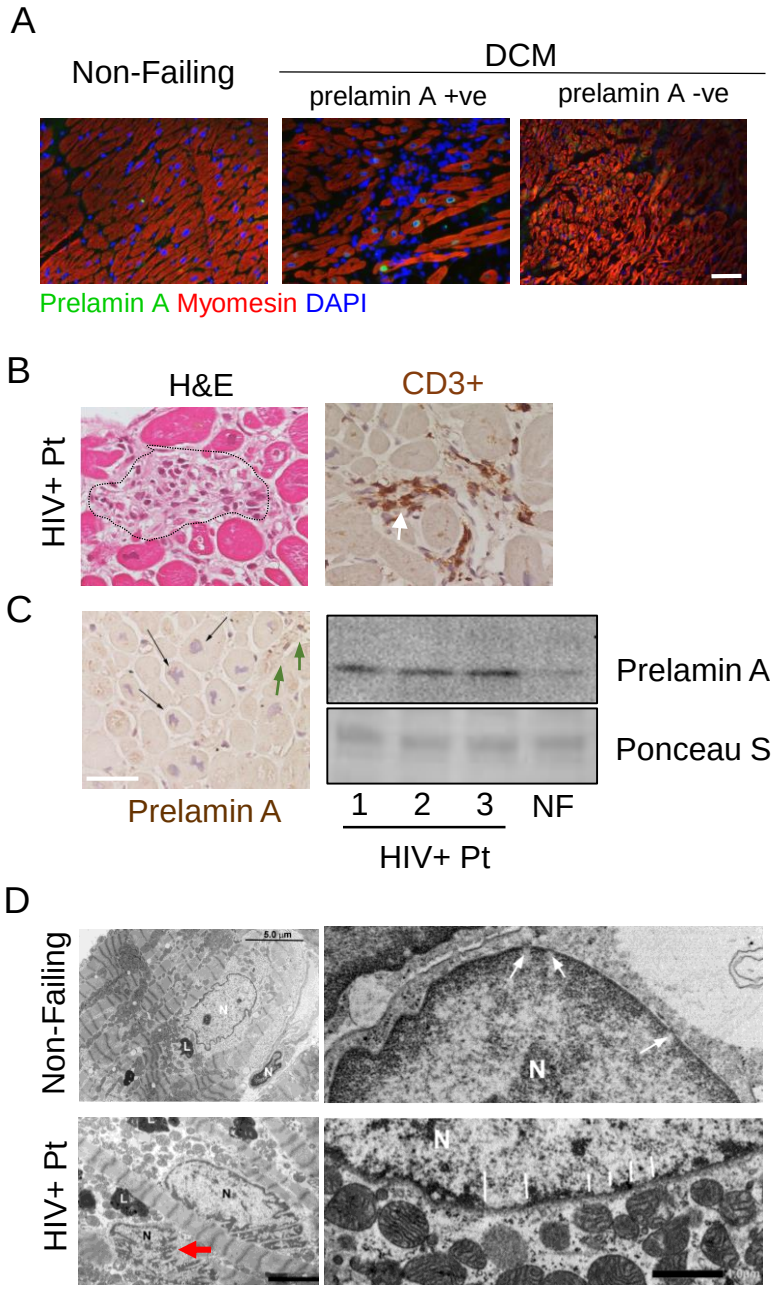

Figure 9. Prelamin A accumulated in hearts of patients with HIV-associated cardiomyopathy under retroviral therapy A. The DCM patient sample in which prelamin A accumulated showed profound mononuclear infiltration unlike other DCM samples. Scale = 40 μm. **B.** H&E and CD3+ immunohistochemistry showing inflammation in HIV+ myocardium consistent with the csPLA-Tg model. Scale = 30μm. **C.** Immunohistochemistry showing focal prelamin A accumulation in CM nuclei (black arrows) and non-CM populations (green arrows) of HIV+ myocardium supported by Western blotting, which detected accumulation of prelamin A in hearts of HIV patients. **D.** Electron micrographs showing nuclear morphology defects in HIV+ myocardium (red arrow, scale = 3 μm) and nuclear pore complexes surrounded by evenly spread heterochromatin in non-diseased myocardium (large white arrows) and heterochromatin displacement in HIV+ myocardium (small white arrows). Scale = 1 μm. N= Nucleus, L=Lipid bodies.

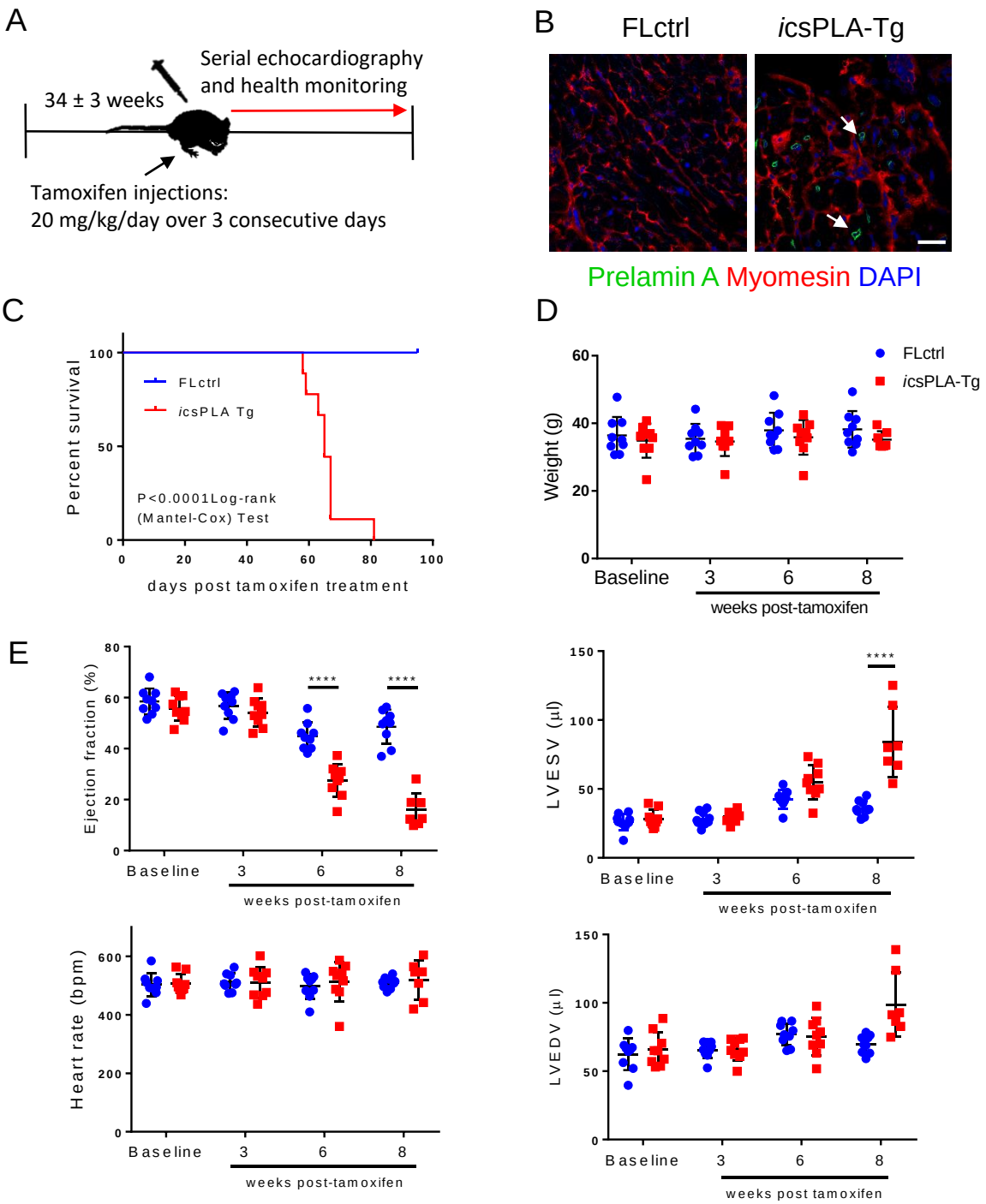

Figure 10. Induction of prelamin A expression in adulthood leads to a progressive and fatal decline in cardiac function in inducible (*i*) csPLA-Tg mice. A. Schematic showing the protocol for assessing the effect of prelamin A acquired in adult mouse myocardium via utilisation of a tamoxifen inducible MerCreMer promoter. **B.** Immunofluorescence staining of heart sections showing the expression of prelamin A in cardiomyocytes of *i*csPLA-Tg mice. Scale = 20µm. **C.** Kaplan-Meier survival analysis showing that csPLA-Tg male and female mice died early compared to FLctrl counterparts, log-rank Mantel-Cox P<0.0001. N= **D.** Body weights remained constant during the course of the protocol. **E.** Cardiac function declined progressively over the course of the protocol. Values are mean ± SD. N = 9- 8 males and 1 female/group. Two-way ANOVA with repeated measures and Sidak's test for multiple comparisons was performed. ****P<0.0001. **F.** H&E and picrosirius red staining showed myocardial disarray and fibrosis respectively. Scale = 30µm.

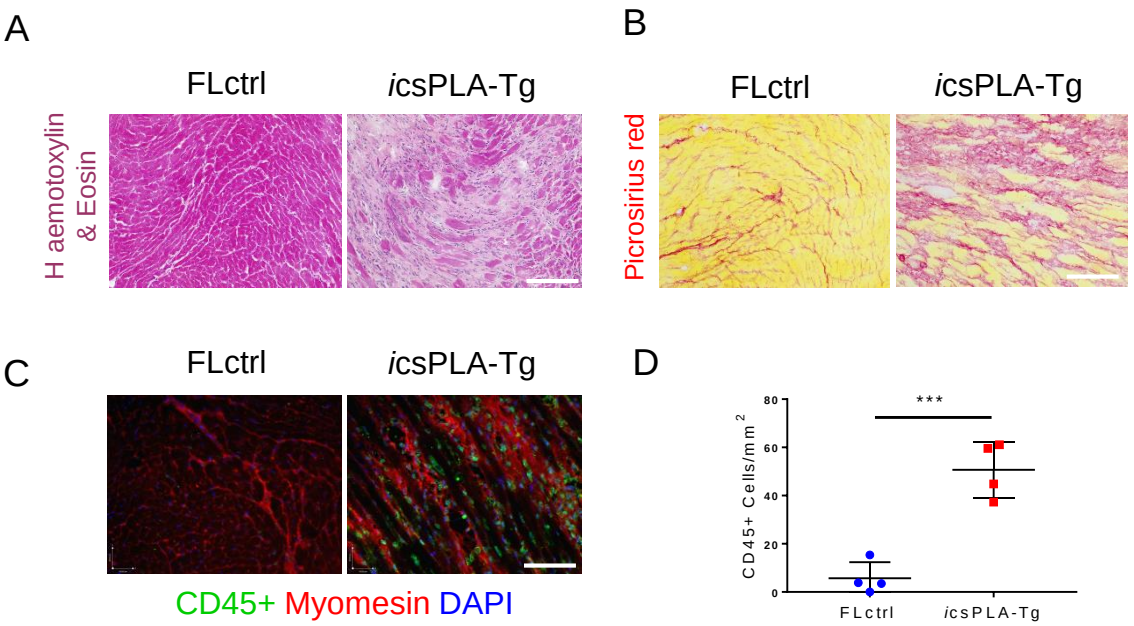

Figure 11. Induction of prelamin A in mouse hearts induces cardiac remodelling and inflammation. A. Haemotoxylin and Eosin and **B.** Picrosirius red staining showed myocardial disarray and fibrosis respectively. **C.** Immunoflourescence micrographs showing CD45+ cells were evident in *ic*sPLA-Tg myocardium. Scales = 30µm **D.** Quantification of CD45+ cells showing an increase in leukocyte population in *ic*sPLA-Tg myocardium. Values are mean ± SD N= 4 males/group. Unpaired student's T-test was performed. ***P<0.001.

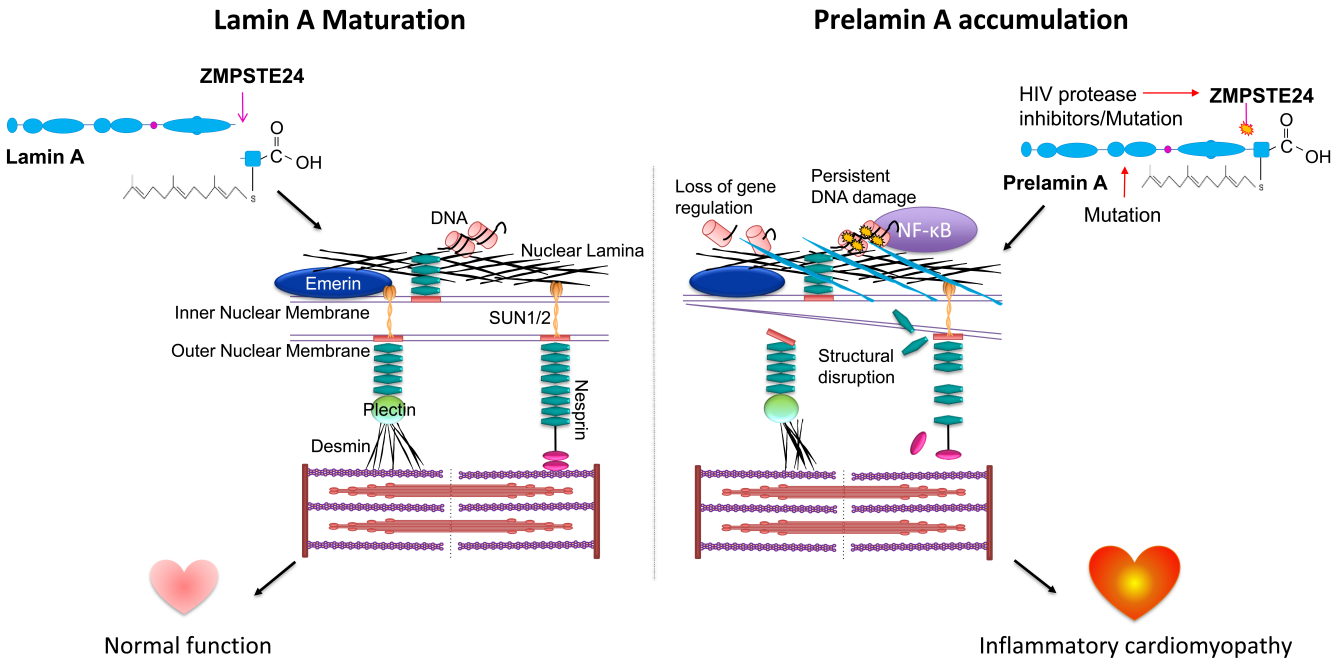

Summary Figure.Schematic showing molecular and phenotypic implications of prelamin A accumulation in the heart. In a normally functioning heart prelamin A is cleaved by ZMPSTE24 leading to laminA insertion in the nuclear lamina. Prelamin A accumulation may occur by mutations in *LMNA*and *ZMPSTE24*genes, and also by inhibition of ZMPSTE24 by HIV protease inhibitors. In this setting prelamin Aaccumulation is likely to contribute to the development of inflammatory cardiomyopathy. In the case of HIV PI inhibitonof ZMPSTE24, switichingtreatmentsto the recently non-nucleoside reverse transcriptase inhibitors (NNRTI's) such asthe recently developed rilvipirine and where necessary, selectingHIV PIs with low-or no affinity to ZMPSTE24 may prove beneficial.